THE PENNSYLVANIA STATE UNIVERSITY
SCHREYER HONORS COLLEGE

DEPARTMENT OF AEROSPACE ENGINEERING

STABILITY AND CONTROL ANALYSIS OF A HUMAN POWERED AIRCRAFT

PETER M. BLASCO
SPRING 2013

A thesis
submitted in partial fulfillment
of the requirements
for a baccalaureate degree
in Aerospace Engineering
with honors in Aerospace Engineering

Reviewed and approved* by the following:

Mark D. Maughmer
Professor of Aerospace Engineering
Thesis Supervisor and Honors Adviser

Joseph F. Horn
Associate Professor of Aerospace Engineering
Faculty Reader

George A. Lesieutre
Professor of Aerospace Engineering
Head of the Department of Aerospace Engineering

* Signatures are on file in the Schreyer Honors College.

ABSTRACT

The Royal Aeronautical Society currently offers a reward entitled the Kremer Prize to the first team to fly a specific mission using a human powered aircraft. The flight course and special requirements of this mission create a unique design challenge in that the aircraft must be fast and maneuverable while still flying solely under human power. A team from Penn State has designed and fabricated an aircraft for this mission. Initial performance estimates determined the design of the aircraft, but a more detailed analysis of the stability and control is necessary to ensure that the aircraft can successfully complete the mission. The stability and control characteristics of this aircraft are presented in tandem with the flight path control requirements. This stability analysis includes calculation of performance characteristics of the aircraft, flight path analysis to find maneuverability requirements, and a stability study to prove aircraft maneuverability. Dihedral of the flexible wing is found to provide critical stability characteristics to make required turns without the use of ailerons. The results of the analysis validate the aircraft's ability to complete the Kremer Prize mission.

TABLE OF CONTENTS

LIST OF FIGURES

LIST OF TABLES

ACKNOWLEDGEMENTS

I would like to acknowledge Dr. Mark Maughmer for advising me on this study and also for all of his work on the *Zephyrus* for the past six years. His efforts have made everything involving the *Zephyrus* possible and this paper would not exist without him. I'd also like to acknowledge Davide Conte for his help with the drag buildup of the *Zephyrus*. Davide and the other members of the flight dynamics team contributed a significant amount of work to the performance analyses of the *Zephyrus*. The other members who contributed as part of the flight dynamics team are Tom Letarte, Collin Russo, Mitch Gennocro, and Yande Liu. I would also like to thank Ben Pipenberg for his help on all things related to the *Zephyrus* as well as his help given to me when writing this thesis. I also acknowledge Blaine Rawdon for his assistance in determining a physical understanding of the stability characteristics of this aircraft. I would finally like to acknowledge all students who were a part of the *Zephyrus* team. Those students span at least five years and have worked very hard to make this aircraft a reality.

Chapter 1

Introduction

The study of this thesis is mainly concerned with the performance and control feasibility of a human powered aircraft designed for a specific mission. This mission exists in The Kremer International Sporting Aircraft Competition sponsored by the Royal Aeronautical Society (RAeS) (4). This competition offers a £100,000 prize to the first team to design, fabricate, and fly a human powered aircraft for a specified purpose. The mission studied in this paper incorporates wind speed as a strict element of the mission requirements. The addition of this element is critical to the mission analysis and design of a human powered aircraft capable of winning the Kremer Prize.

A team of Penn State engineers began the design and fabrication of an aircraft to complete the Kremer mission starting in 2008. This team is composed of undergraduate members of the Flight Vehicle Design and Fabrication course which is more affectionately known as "sailplane." Taught and advised by Dr. Mark Maughmer, the sailplane course provides an enormous learning opportunity for students who enjoy "hands on" work. Students are allowed to take the course in their freshman year and continue every semester up until graduation. This allows unique and course related information to be passed along by upperclassmen to lowerclassmen as they work together towards common project goals. The author of this thesis began working on the human powered aircraft project as a freshman and is now the project leader. Although a significant amount of work and analysis (a large amount done by this author) has contributed to the design and fabrication of this aircraft, this thesis will not present that work

in detail. It will instead focus on the flight path analysis and stability properties of the aircraft as dictated by the mission requirements.

Historical Perspective of Human Powered Design

A rich history of aerodynamic performance calculation, technological advancement, and design ingenuity exists in the history of human powered aircraft (HPA). The thrilling stories of attempted human powered flight are often accompanied by rigorous studies into aerodynamics, lightweight materials, and the unique stability characteristics of these HPAs. There is much to learn from the successes and failures of the founders of human powered flight.

Although the first attempts at human powered flight date back to 1783, popularity of the cause was not present until the advent of the first Kremer Prize in 1959. Henry Kremer, a business man and member of the RAeS, offered this prize of £5000 to the first group to design, build, and fly an aircraft about a half-mile figure eight. Interest in the UK immediately spiked and many competitors attempted the Kremer challenge. However, the period from 1959 to 1976 was dominated by heavy aircraft that had very similar designs to sailplanes at the time. Many designers such as SUMPAC, Brian Kerry, and Chris Roper attempted to refine aerodynamics without looking at the HPA problem from an entirely open perspective. All of their respective HPAs flew, but none of them were light enough to sustain flight for long periods of time and most importantly none of them could perform a sustained turn. This was partially due to the increases in drag during turn and partially due to the lateral instability of the large span aircraft (1). This historical fact is a motivating factor of the work presented in this thesis. The HPA's ability to turn is critical to the mission. A major goal of this thesis is to prove that the aircraft designed by the sailplane class does have the required ability to turn.

In 1976, the HPA problem was gazed upon by a new competitor. Paul MacCready, a former world-championship glider pilot, looked at the Kremer challenge from an entirely new perspective. Rather than focus on designing by aerodynamics to reduce the drag, MacCready instead focused on the power requirements created by drag in their purest form. He hypothesized that the best way to reduce the drag and power required on an aircraft was to make it cruise at the slowest speed possible. This simple new idea was the key to HPA design and has been a staple of HPA design ever since it was first introduced. MacCready proved his ingenuity by winning the first and second Kremer prizes in 1977 and 1978 respectively with his *Gossamer* aircraft (Figure 1-1). Ever since the winning of the first Kremer prize, teams from all over the world have designed and continue to design HPAs for the Kremer competitions and for personal goals (1).

Figure 1-1. The *Gossamer Albatross*. This is an image of the *Gossamer Albatross* crossing the English Channel on its way to win the second Kremer prize in 1978. *http://www.avinc.com/img/media_gallery/Gen_GossamerAlbatros*

Advances in composite fabrication technology and understanding of low speed aerodynamics have led to the design and fabrication of HPAs in today's generation. These aircraft

are extremely light and capable of amazing feats. However, they would be nothing without the important knowledge learned about speed, power, and stability from the success and failure of past HPAs. Turning has always been a large problem for HPAs. This thesis intends to fully study the turning capabilities of an already designed HPA and prove that a pilot is capable of controlling the HPA in a winning Kremer prize flight.

The Kremer Competition for Sporting Aircraft

The Kremer Prize mission is key to providing the design and stability requirements of the HPA. The mission is the timing of two flights: one clockwise and one counter-clockwise about the mission course (Figure 1-2). The two flight times are added and the total time must be less than seven minutes. The aircraft must takeoff and then fly across the start line (at any direction) at a minimum altitude of 5.0 meters at which point the first official flight time starts. The first official flight time ends when the aircraft crosses the respective finish line at an altitude of at least 5.0 meters. The same starting and finishing rules apply to the second flight and there can be a maximum one hour of time between flights. The most important rules of the competition are that the wind speed must not fall below 5.0 m/s for more than 20 seconds during an official flight and the mean wind speed for the total duration of the flights must be above 5.0 m/s. These rules set an important design constraint which is that the minimum speed required to complete the course is roughly 19.5 knots (8). The specific rules and guidelines for the Kremer Competition for Sporting Aircraft are given in reference 8.

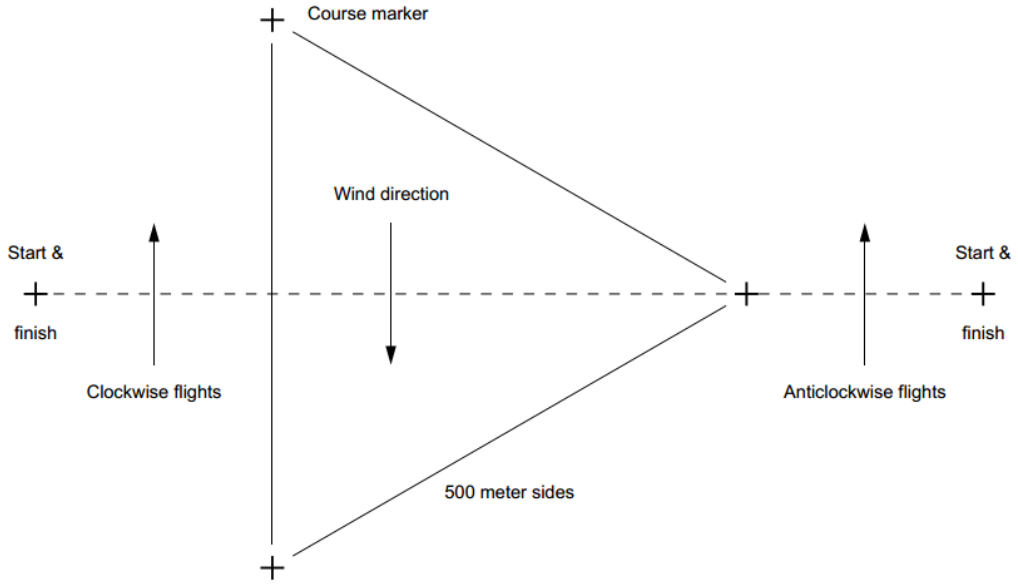

Figure 1-2. Kremer Competition Official Course. Note that the first official flight is flown clockwise and the second official flight is flown anticlockwise. See reference 8 for more details regarding the Kremer mission requirements.

Chapter 2

Penn State's *Zephyrus* Human Powered Aircraft

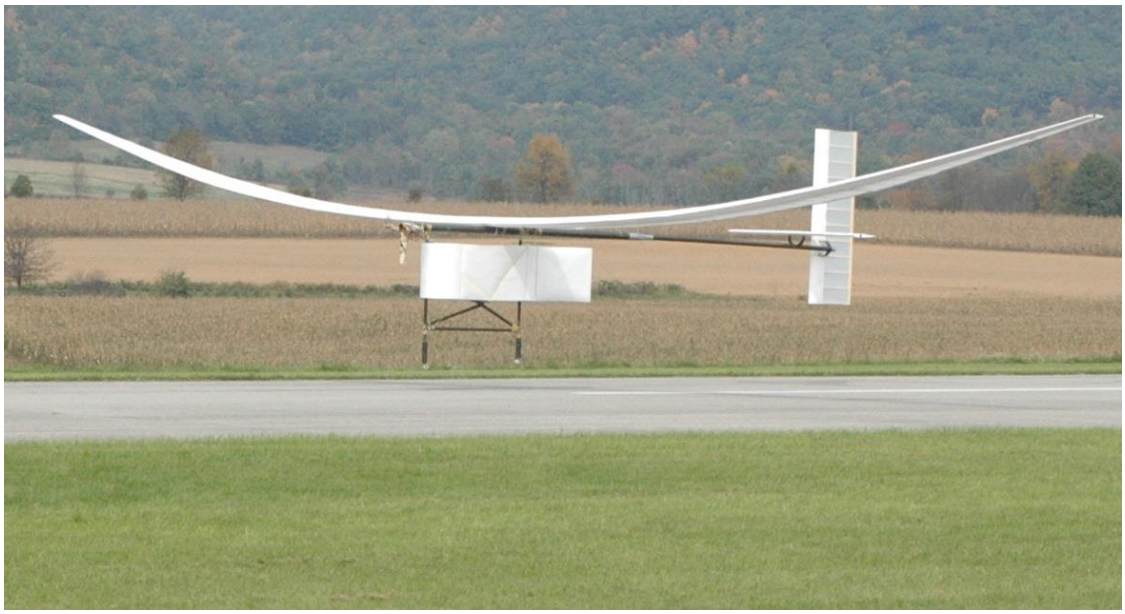

Figure 2-1. *Zephyrus* Flight Test Photo. Flown with 140 lb ballast and under radio control. This flight test took place in the spring of 2012.

The initial design of a HPA to complete the Kremer mission was completed by sailplane students in 2009. However, note that design changes from the initial design have been ongoing and are still present in 2013 as more information is gained from flight testing and part fabrication. The aircraft parameters and performance data displayed here are up to date as of March 2013. The aircraft was named the PSU *Zephyrus* by the original designing class and will be referred to by that name throughout this thesis. The early designs of the *Zephyrus* were performed using historical HPA design methodology. The aircraft was designed to be as light as possible and as slow as possible in order to reduce powered required. However, the aircraft design was also constrained by the requirement to fly fast enough to complete the mission. A rough cruising speed estimate of 12 m/s (24 knots) was made at the time of the first design. As designs solidified in early 2010, fabrication of aircraft parts began and was carried out up until the present date. The

first prototype version of the aircraft was finished and test flown in the spring of 2011. This version did not include a fuselage, was un-ballasted for pilot weight, and was propelled by electric motor propellers. The next test flight of this prototype flew in the spring of 2012 and included the addition of 140 lbs. ballast in a temporary fuselage fairing to simulate the weight of a pilot. This test flight was a simple straight and level flight at low altitude and was not flown under human power. Figure 2-1 shows a photo of this ballasted flight test. The aircraft is now in the final fabrication stages and ready for a turning flight test. The potential for crashes during turn and inability to turn are motivations for the analysis presented herein. The findings of this thesis will help dictate the turning maneuvers performed in flight test three.

Aircraft Parameters

The aircraft parameters were found by design and verified after fabrication. Table 1-1 gives important aircraft parameter information that will be used in stability and performance calculations. The parameters in Table 1-1 are given in English units in order to be consistent and have a practical meaning. However, the mission requirements are given in SI units and thus made some calculations easier when performed using SI units. The author of this thesis has a list of the Table 1-1 parameters in SI units as well to ensure accuracy in calculations. Figure 2-2 shows a side view of the most current aircraft design. All parameters are relevant to the most recent version of the aircraft.

Table 1-1. *Zephyrus* Parameters

Aircraft	Wing	Horizontal Tail	Vertical Tail
W_{gross} = 208 lbs	S = 163.7 ft²	S_{ht} = 12.64 ft²	S_{vt} = 15.89 ft²
V_{stall} = 27 ft/s	c = 2.37 ft	c_{ht} = 1.47 ft	c_{vt} = 2.17 ft
h_n= 0.48	b = 73.8 ft	l_t = 15.5 ft	$\delta_{r,max}$ = 39.4º
V_H= 0.507	a_{wb} = 5.73 /rad	a_{ht} = 4.297 /rad	b_{vt} = 7.33 ft
$\frac{\partial \epsilon}{\partial \alpha} = 0.14$	$h_{n,wb}$ = 0.17	$\delta_{e,max}$ = 22.5º	a_{vt} = 4.297 /rad
		b_{ht} = 8.67 ft	

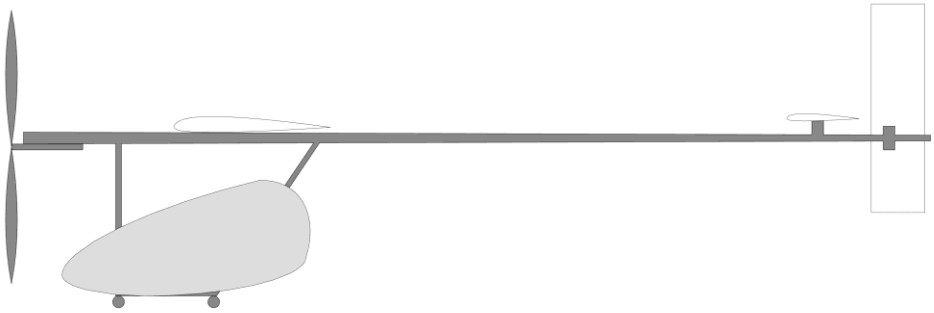

Figure 2-2. *Zephyrus* Side View. This view of the aircraft is representative of the final design before flight test three.

Zephyrus Performance Estimates

A starting point for this analysis is calculating the power required as a function of airspeed. Comparing the power required to the pilot's available power gives a cruise airspeed range necessary for later use. In order to accurately find power required, the drag must first be calculated.

Calculating the *Zephyrus* Drag

A drag buildup of the *Zephyrus* is performed using Equations (1) through (4). The drag build-up starts at stall speed and calculates drag at 1 ft/s increments up to 47 ft/s. Using Equation (2) and trim drag calculations, C_Ls are calculated for the wing and horizontal tail (3).

$$D = 1.05 * (D_{Wing} + D_{HT} + D_{VT} + D_{Fuse}) \quad (1)$$

$$C_L = \frac{2W_{gross}}{\rho V^2 S} \quad (2)$$

The 1.05 in Equation (1) represents an addition of 5% to the total drag to account for interference drag. Equation (3) shows how the wing, horizontal tail, and vertical tail drag is calculated where *x* is a subscript represented by the wing or tails. For this drag buildup, profile drag coefficients are found by interpolating drag coefficients from C_l vs. C_d tables obtained using XFOIL. The wind profile drag in particular includes drag coefficient calculation for varying Reynolds number between the root and tip chord. The half span is split into three sections in order to account for changes in profile drag due to low Reynolds number effects. Note that induced drag for the vertical tail is zero.

$$D_x = \frac{1}{2}\,\rho V^2 S_x (C_{D,prof\ x} + C_{D,i\ x}) \quad (3)$$

$$C_{D,i\ x} = \frac{C_{L\ x}^2}{\pi e AR} \quad (4)$$

The last component of drag is contributed by the fuselage. The drag on the fuselage is calculated as if it is a vertical lifting surface in which the induced drag is always zero. Therefore the profile drag calculation is all that is necessary and is done by modeling the fuselage as four separate sections with varying chords and different NACA airfoils. These airfoils provide the profile drag coefficients necessary to calculate the fuselage drag. Figure 2-3 shows a plot of the drag calculated in Equation (1) vs. airspeed. This plot is important because it gives the minimum drag speed in cruise condition which is roughly 21 knots. This is a good initial result because the minimum drag speed is higher than the estimated minimum mission speed of 19.5 knots.

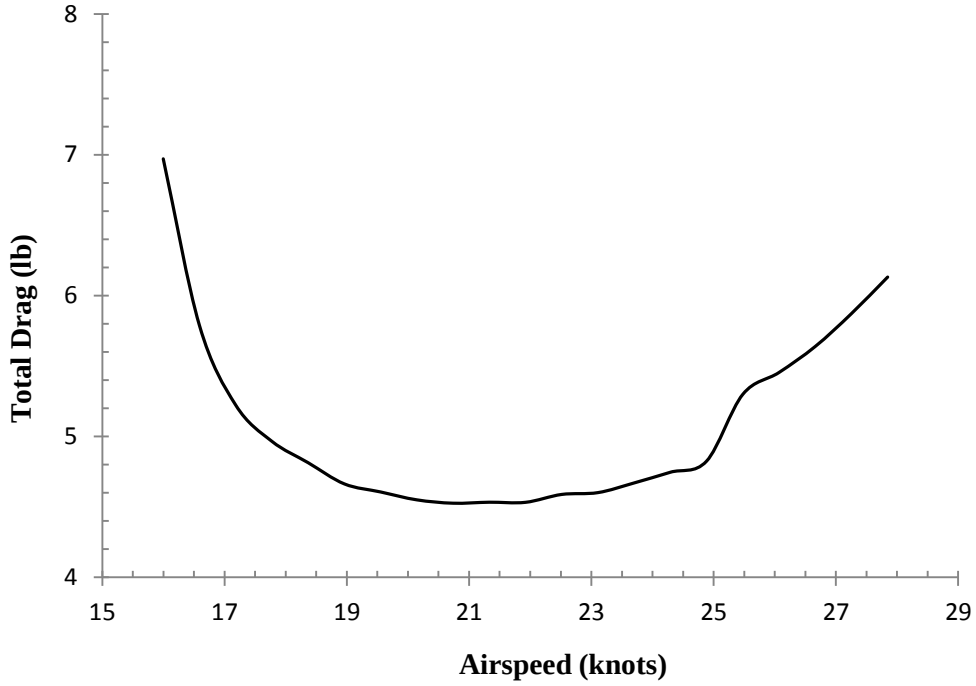

Figure 2-3. *Zephyrus* Drag vs. Airspeed. This drag curve is for straight and level flight and displays a minimum drag range of 19 to 24 knots.

Drag Considerations when Turning

The drag plot in Figure 2-3 is a useful resource for computing power required in steady level flight, but is not absolute for lateral flight attitudes until the increased drag on the aircraft during a turn is analyzed. When in a coordinated turn, an aircraft has to produce more lift and therefore more drag. The lift coefficient calculated in Equation (2) changes by adding in a term for bank (9). This bank angle term shown in Equation (5) increases the lift coefficient at a given airspeed and typically shifts the drag curve up and to the right.

$$C_L = \frac{2W_{gross}}{\rho V^2 S \cos(\Phi)} \tag{5}$$

The relationship between C_L and C_D in this case is such that a percentage increase in C_L gives a nearly equivalent increase in C_D. This assumption is supported by the equations in reference 9 and verified by the results of a turning drag study that is independent of the *Zephyrus* project. Figure 2-4 shows the results of the independent study which is the calculation of turning drag for a *Ventus 2C* sailplane. The *Ventus 2C* has similar aerodynamic and geometric properties to the *Zephyrus* and is therefore suitable for studying the increase of drag in turns. The drag on the *Ventus 2C* is also calculated in the exact same way as it is on the *Zephyrus* (see Appendix A for MATLAB codes).

An important finding made later in this thesis is that the *Zephyrus* is unlikely to encounter bank angles of more than 15º. The increase in drag from a 15º angle of bank is roughly 4% (Figure 2-4). This is so minimal that the drag increase in coordinated turns at bank angles less than 15º can be neglected in this study. The amount of extra power that the pilot must output is easily manageable at less than 4%. This conclusion is useful when analyzing the mission cruise speed in both straight and turning flight. However, it is important to note that a drag increase is likely to come from uncoordinated turns in the aircraft. This drag increase is difficult to predict and an assumption is made that the pilot will be able to overcome it.

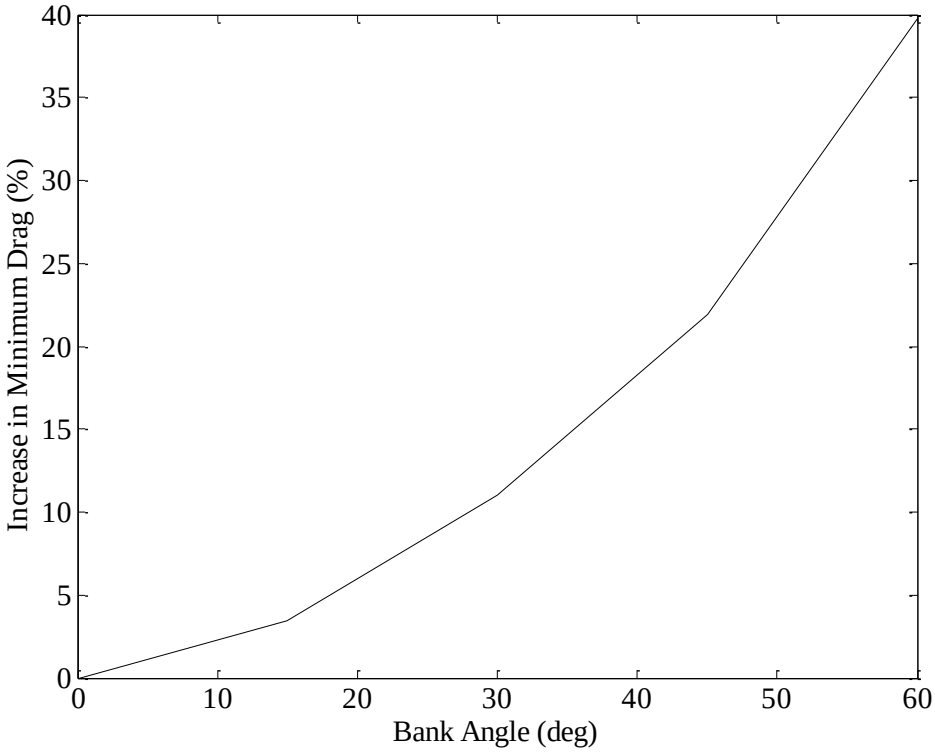

Figure 2-4. *Ventus 2C* Drag Increase vs. Bank Angle. This plot is from a study of the *Ventus 2C* sailplane. The relationship between bank angle and drag is very similar to what it would be on the *Zephyrus*.

Estimating Power Required

The results of the drag calculations in the previous section are used to find power required using Equation (6). Power available is assumed to be 282 Watts on the basis that a pilot can output 350 Watts and assumptions can be made for shaft efficiency and propeller efficiency. This analysis is only concerned with the cruise speed range in which propeller efficiency will be maximized, so accuracy is still maintained by assuming power available is constant. The pilot output power is multiplied by a shaft efficiency of 0.95 and propeller efficiency of 0.85 to give power available. These values are estimated assumptions for mechanic and aerodynamic losses. Figure 2-5 shows that the aircraft is able to safely cruise with power available within the 18 to 24

knot range. This is a great result because the minimum course completion speed of 19.5 knots is at the lower end of this range. This range of airspeeds can now be used for further analysis to estimate mission completion times.

$$P_{Req} = DV \tag{6}$$

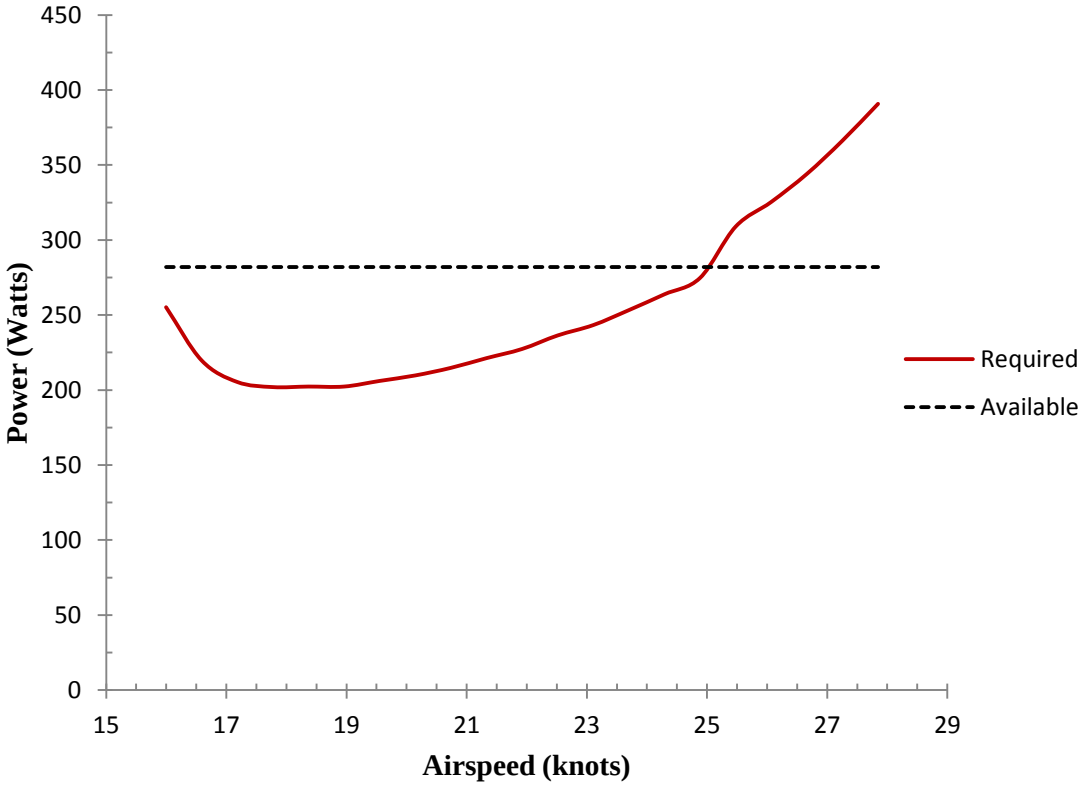

Figure 2-5. *Zephyrus* Total Power vs. Airspeed. Power Available is not exact, but conservative and accurate enough to determine an effective cruise range.

Chapter 3

Flight Path Analysis of the Competition Course

Before beginning a stability analysis, it is necessary to have some definitions for maneuverability. An analysis of the competition flight path can give the specific turn rates and speed that this aircraft has to fly at in order to complete the course on time. These values will be important for stability analyses and also provide insight to the most important factors of mission performance. The following section gives detailed information about a MATLAB simulation that estimates the time to complete the Kremer mission given a set of input constraints that are wind speed, aircraft cruising speed, and bank angle. The input constraints are partially determined by analysis and partially by intuition. The aircraft cruising speed range is determined entirely by the performance analysis in the previous section. However, wind speed is guessed to range between 5.0 m/s and 7.0 m/s. This guess is assuming a maximum wind speed of 7.0 m/s simply because the aircraft is not likely to compete for the mission at any speed above 7.0 m/s. The bank angle range is guessed by constraining the maximum bank angle to 25º.

Any bank above 25º can be considered unsafe and is a major cause of other HPA crashes in the past (5). This is because a high bank angle at low speed is accompanied by a small turning radius. This small turn radius wouldn't be an issue for most aircraft, but it is for HPAs because of their large span. The difference in local air velocity at either wing tip creates a lift differential across the span of the wing that tends to roll the aircraft inward. This is especially prevalent at high C_Ls. At high bank angles and low speed, this roll moment can become large enough to where the inward roll is unrecoverable. To be absolutely safe, the *Zephyrus* will never attempt a banked turn of more than 25º (preferably less) regardless of intuitive or analytical results.

MATLAB Time Estimation Simulation

The solution of time estimated to complete the course is complex mainly because of the addition of the wind vector to the cruise airspeed vector as the aircraft flies. This simulation must find the ground speed and ground heading such that the ground heading of the aircraft matches the direction of the course path. This can be done by constraining the direction of the ground speed vector and solving for ground speed using simple trigonometry and vector addition. There are two major solutions in this time estimation simulation. The first estimates the time that it takes to turn using a numerical integration method. The turning algorithm also solves for the ground tracking in turns at constant bank angle and plots this information for each turn. The second solution calculates the time that is takes to fly each straight leg using the vector calculation methods described earlier. Both solutions are combined to finally give the total time to complete the Kremer course.

Turning Algorithm

This simulation estimates the turning time and ground track by finding the ground speed and heading of an object performing a 360º turn about a point. Cruise speed remains constant for this object and is always tangent to the circle. Wind speed is constant and always in the downward direction. Figure 3-1 gives a visual representation of what speeds and angles the simulation is calculating. An *x* and *y* coordinate system is established to help calculate the vector components of the ground track velocities.

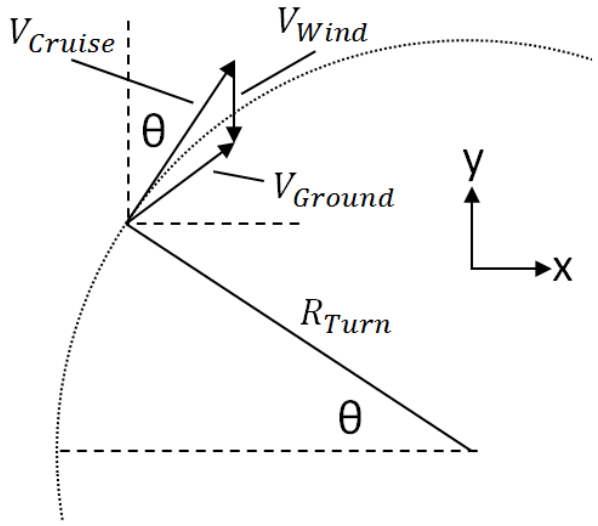

Figure 3-1. Visualizing Turn Simulation Approach. The simulation calculates the turning ground speed vector by finding the ground velocity vector for an object turning 360° about a point. The ground track will be different than the circle, but the time to complete the full turn will be accurate.

This first part of the algorithm solves for the ground track velocities using Equations (7) through (9). The angle θ is the turning angle which conveniently provides positive and negative values for the cruise velocity direction in *x* and *y* via the sine and cosine functions in Equations (8) and (9).

$$R_{Turn} = \frac{V_{Cruise}^2}{g\tan(\Phi)} \tag{7}$$

$$V_X = V_{Cruise} sin(\theta) \tag{8}$$

$$V_Y = V_{Cruise} cos(\theta) - V_{Wind} \tag{9}$$

The next step in the algorithm is to numerically integrate values for V_X and V_Y over time around the circle. This is done using a simple numerical integration shown in Equations (11) and (12). An interesting fact is that the total time to complete the turns only depends on turn radius and cruise speed. The wind speed does not affect the time to turn, but instead affects the ground

tracking of the turn. This is because the apparent loss of ground in the turning simulation will be nonexistent in the Kremer course flight path. In fact, the extra ground covered in tailwind turns will actually subtract from the straight legs of the course. The total time to complete the 360° of turns about the first clockwise lap is shown in Eq. (10). This is used to solve for the total course time as well as the integration time step *dt*. Equation (13) is necessary because it solves for the total length of the turning ground track. This value will be used later to help solve for accurate straight leg distances.

$$T = \frac{2\pi R_{Turn}}{V_{Cruise}} \tag{10}$$

$$X_{i+1} = X_i + V_{x,i}dt \tag{11}$$

$$Y_{i+1} = Y_i + V_{y,i}dt \tag{12}$$

$$L = L_i + \sqrt{(X_{i+1} - X_i)^2 + (Y_{i+1} - Y_i)^2} \tag{13}$$

An example ground track at a given cruise speed, bank angle, and wind speed is displayed in Figure 3-2. This figure shows that the ground track takes up a significant amount of space and puts the aircraft far away from where it started. As already discussed, this displacement of position does not affect the total time by a large amount.

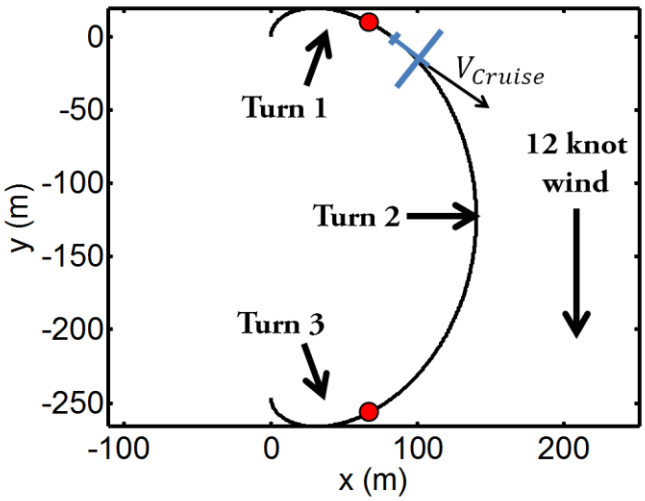

Figure 3-2. Turning Ground Track. This is a plot of the 360 degree turn flight path given a 12 knot wind, 21 knot airspeed, and 10 degree angle of bank. The red dots represent breaks between where each turn would take place on the triangle course. Turn two is the largest and is nearly a 180 degree turn.

An important side result of the turning algorithm is the plotting of ground path when turning at constant bank angle in the wind. It is useful to find the entry and exit point of each turn of the Kremer course so that each turn can be individually plotted and analyzed by the pilot in the future. This is done by calculating geometrical relationships between the ground speed heading and aircraft heading (calculations in the next section). The simple geometry is applied to the angles about the circle and each turn is individually separated by time and ground track. Using Figure 3-8 as a reference, Figures 3-3 through 3-7 show the ground tracking path at a 15º bank for every turn encountered in the clockwise and counterclockwise laps of the course.

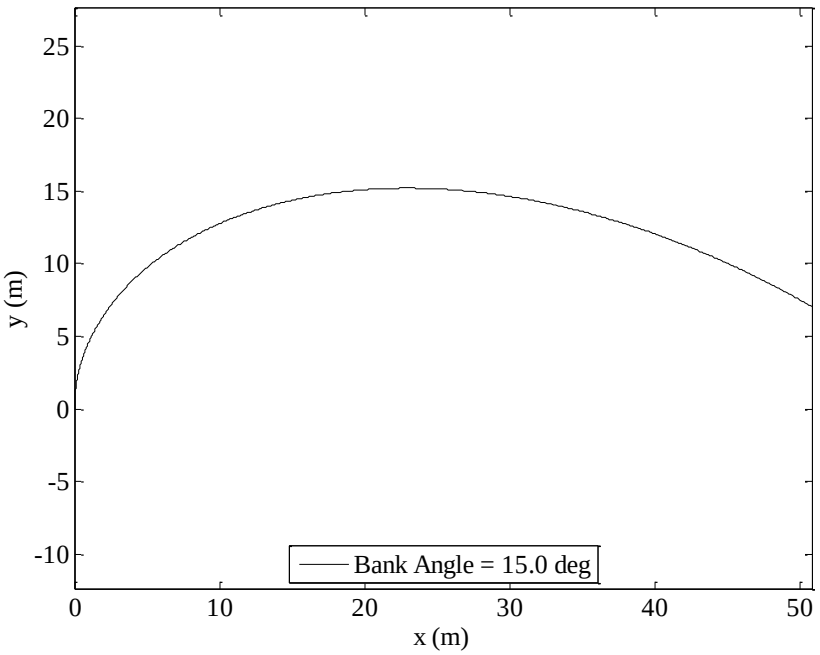

Figure 3-3. Turn One Ground Flight Path Track. Simulation is run at a cruise speed of 22 knots, bank angle of 15º, and wind speed of 6 m/s.

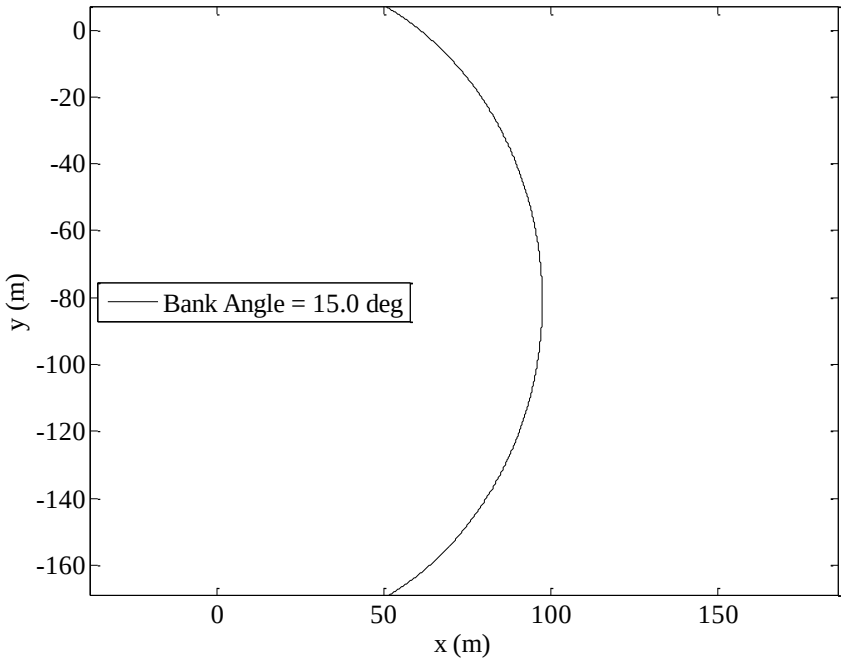

Figure 3-4. Turn Two Ground Flight Path Track. Simulation is run at a cruise speed of 22 knots, bank angle of 15º, and wind speed of 6 m/s.

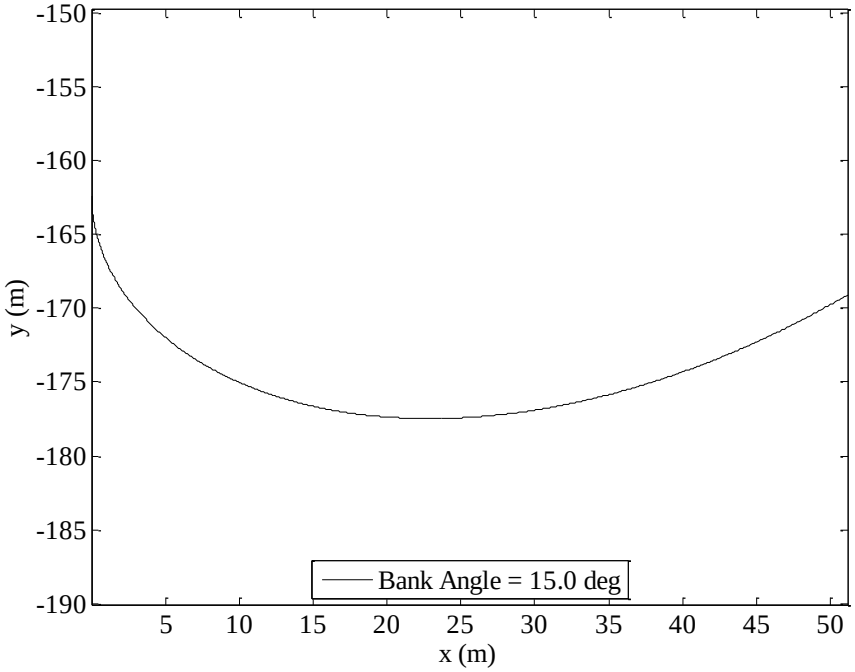

Figure 3-5. Turn Three Ground Flight Path Track. Simulation is run at a cruise speed of 22 knots, bank angle of 15º, and wind speed of 6 m/s.

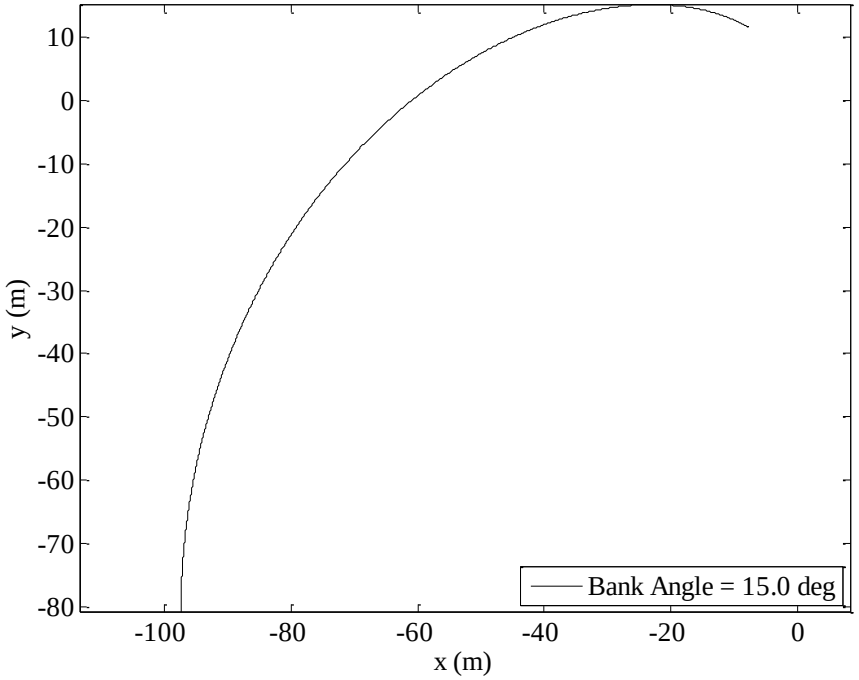

Figure 3-6. Turn Four Ground Flight Path Track. Simulation is run at a cruise speed of 22 knots, bank angle of 15º, and wind speed of 6 m/s.

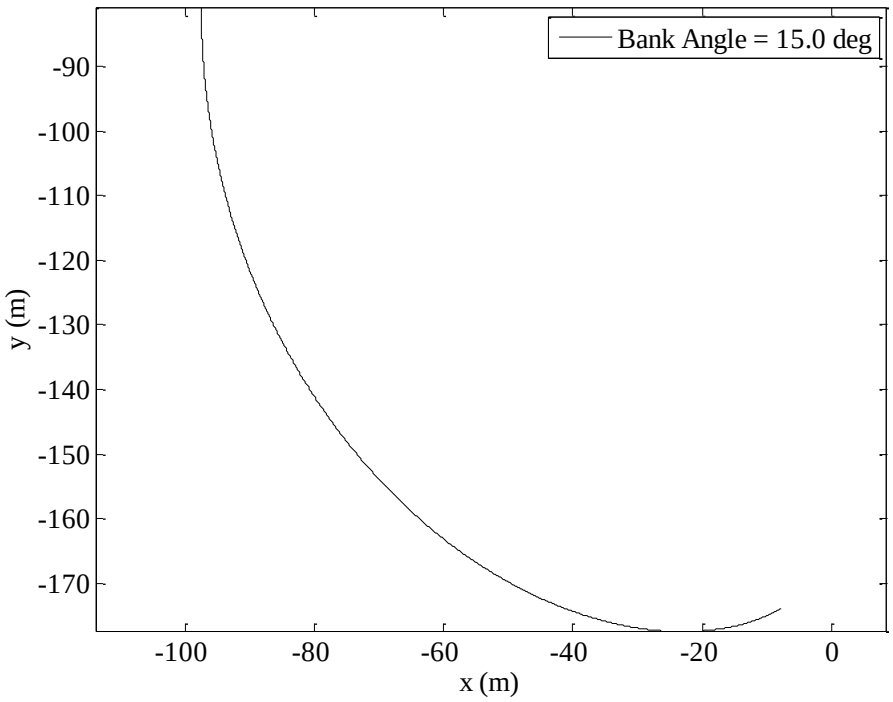

Figure 3-7. Turn Five Ground Flight Path Track. Simulation is run at a cruise speed of 22 knots, bank angle of 15º, and wind speed of 6 m/s.

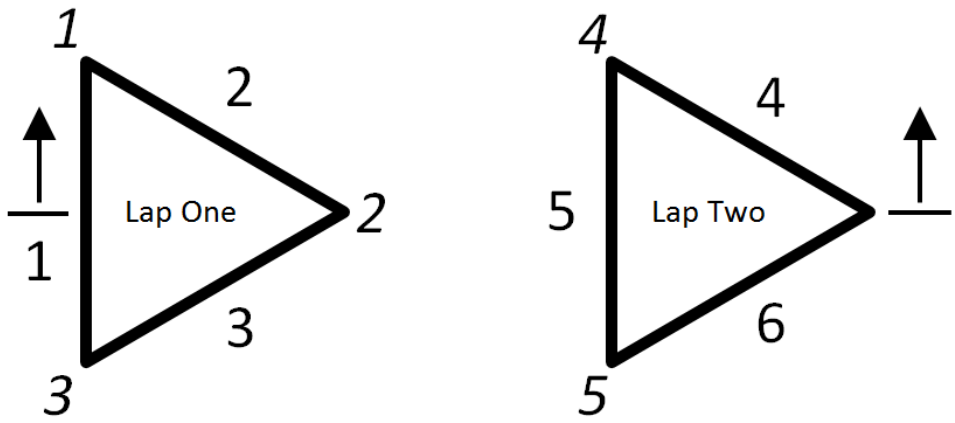

Figure 3-8. Kremer Course Diagram. This figure gives nomenclature values to the various course legs and turns. Course legs are denoted by a normal number whereas course turns are denoted by an italicized number.

Straight Path Algorithm

The solution of straight path times is determined by the vector relationships between the cruise vector and the ground speed vector. This is a simple relationship for the legs parallel to the wind vector. However, the angled leg times are more difficult to solve. The ground speed is solved for a specific heading of 60° from the *y* axis in either direction. This is done using Equations (14) through (16). This gives an interesting result when analyzing the ground speed of two opposing legs on the same lap (legs 2 and 3 or 4 and 6). Even though the *x* component of velocity is in the opposite direction for each leg, the magnitude of those *x* velocities are equivalent. The direction and magnitude of the *y* velocities are equivalent, so therefore the magnitude of the ground speed is equivalent for the two legs and their traversal times are also equivalent. In terms of the aircraft ground speed, the two angled legs of the clockwise lap (legs 2 and 3) are characterized by a headwind and the two legs of the counter-clockwise lap (legs 4 and 6) by a tailwind.

$$V_{X,G} = \frac{\pm 2V_{Wind}\tan(\theta_C) + \sqrt{\left(2V_{Wind}\tan(\theta_C)\right)^2 - 4(1+\tan^2(\theta_C))(V_{Wind}^2 - V_{Cruise}^2)}}{2\left(1+\tan^2(\theta_C)\right)} \quad (14)$$

$$V_{Y,G} = V_{X,G}\tan(\theta_C) \quad (15)$$

$$V_{Ground\ Speed} = \sqrt{V_{X,G}^2 + V_{Y,G}^2} \quad (16)$$

The leg distances are divided by the ground speed to get the times for the each respective leg. However, the leg distances are not exactly 500 meters because of the turn traversal distances cutting into the leg distances. The leg distances are solved for using Equations (17) and (18) and referencing to Figure 3-8. The time to fly each separate leg is calculated using Equation (19). Finally, the times of every individual turn and leg are added together in Equation (20) to give an accurate total flight time.

$$Ds_2 \; and \; Ds_3 = 500 - \frac{L - 2\pi R_{Turn}}{2} \tag{17}$$

$$Ds_5 = 500 - (L - 2\pi R_{Turn}) \tag{18}$$

$$T_{Leg,i} = \frac{Ds_i}{V_{GS,i}} \tag{19}$$

$$T_{Total} = \sum T_{Turns} + \sum T_{Legs} \tag{20}$$

Constraint Results for Use in Dynamic Simulation

The final results of the time simulation are given in the form of contour plots in Figures 3-9 and 3-10. Each contour plot constrains an individual variable which allows a full spectrum of mission completion times to be displayed referencing the two other variables. This is convenient for making conclusions about the importance of each variable. In Figure 3-9, bank angle is constrained so that wind speed and cruise speed can be analyzed. The completion time of the course is mainly determined by wind speed and cruise speed. There is a linear tradeoff between each of those values that have roughly an equivalent effect on course completion time. The first result is that a winning time is attainable for the Zephyrus at minimum wind speed for the entire cruise range. This encouraging result is the first concrete proof that the Zephyrus can win the Kremer Prize. Assuming a conservative wind speed of 12 knots, Figure 3-9 shows that the Zephyrus can complete the Kremer course with 30 seconds of time remaining if flown at a cruising airspeed of 22 knots. According to the performance analysis in section II, this airspeed is attainable and allows for some excess power available to the pilot for use in turns and climbs.

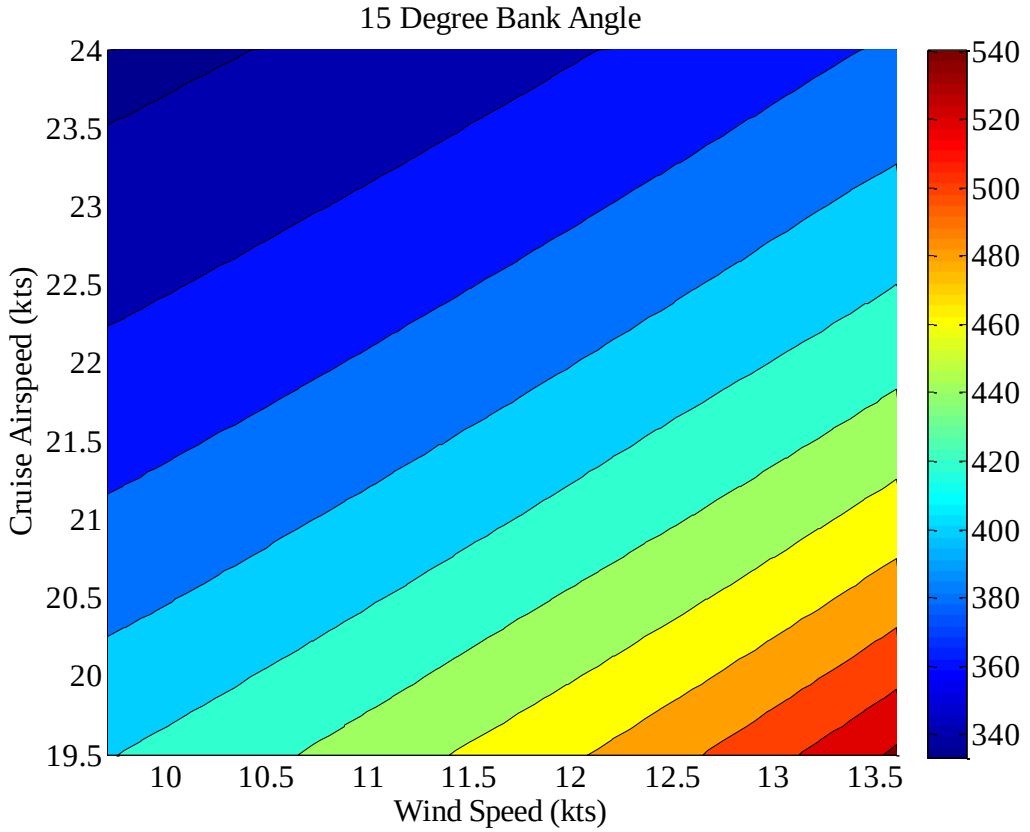

Figure 3-9. Contour Plot of Mission Completion Time. In this case, the bank angle is held constant at 15º to analyze the tradeoffs between wind speed and cruise airspeed.

An interesting conclusion is discovered when analyzing how changes in bank angle affect the mission completion time. Figure 3-10 shows that the mission completion time contours flatten out after bank angles of 15°. This means that decrease in completion time after banks of 15º is practically negligible. This is a fantastic result because of the poor lateral stability properties of HPAs. This analysis provides proof that constraining the lateral motion of the *Zephyrus* to light maneuvers of no more than 15º of bank is an optimal strategy for mission completion. Therefore, a bank angle of 15º will be used as the performing bank angle for all future analyses.

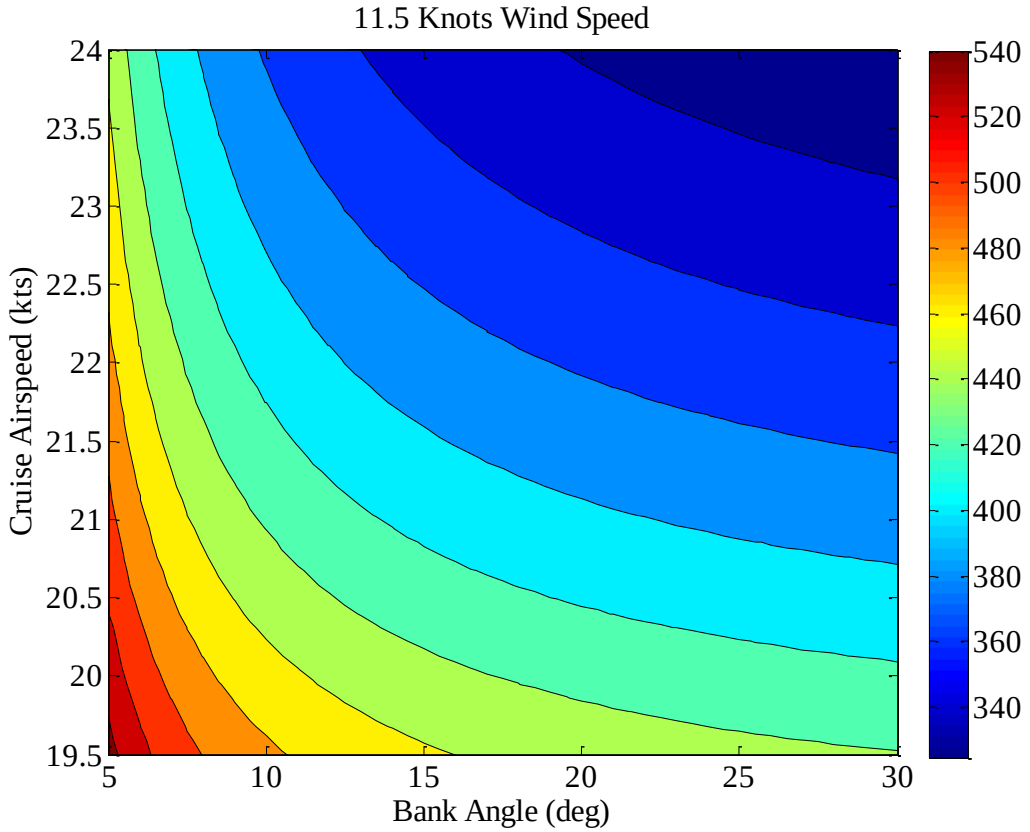

Figure 3-10. Contour Plot of Mission Completion Time. In this case, the wind speed is held constant at 11.5 knots to analyze the tradeoffs between bank angle and cruise airspeed.

The final results of the MATLAB flight path simulation are encouraging. This analysis concludes that the *Zephyrus* is capable of winning at conservative mission conditions and therefore likely to win the Kremer prize in any scenario.

Chapter 4

Stability and Control of the *Zephyrus* Aircraft

The stability and control properties of the *Zephyrus* are critical factors in determining if the aircraft is capable of winning the Kremer prize. The aircraft must be safe and controllable given the flight conditions of 22 knots cruising speed and 15º banked turns. The relative meaning of "safe and controllable" is something that must be defined. In the case of this aircraft, the turning scenario will be safe as long as the aircraft can trim in a 15º bank without large sideslip angles. This is analyzed using a lateral static stability model. The lateral static stability trim model will also be used to find a relationship between bank angle and trimming requirements (sideslip, rudder deflection, and yaw rate). The results of these relationships will also help in determining dangerous flight attitudes.

The dynamic aircraft response between level flight and banked turns is important, but something that is very complex and unique for this type of aircraft. The analysis of such a thing is somewhat useless compared to flight testing analyses which are currently in process. There are simply too many factors such as apparent mass and aero-elasticity that contribute to divergences and nonlinearities in dynamic aircraft response. It is instead more useful to look at historic HPA dynamic response and discuss the predicted response along with linear system modes.

Calculating Stability and Control Derivatives

In order to perform stability analyses of the *Zephyrus*, the non-dimensional stability derivatives of the aircraft must first be calculated. The apparent mass effects of the wing, aero-elasticity of structures, and low speed of this aircraft make it extremely difficult to correctly

calculate these derivatives. For this reason, multiple sources and databases are used to calculate and estimate the *Zephyrus* stability derivatives.

Two textbook sources are used to generate equations for derivatives. One of these sources is *Dynamics of Flight: Stability and Control* (3). This text provides equations for most of the stability derivatives, but they are mostly approximations for higher speed generalized aircraft. Many assumptions are made in this text that could possibly result in inaccurate stability derivatives for the Zephyrus. The textbook source used to mitigate these errors provides example calculations for sailplanes (7). The sailplane examples are useful because the HPA can be approximated as having the properties of a sailplane when necessary. The last resort to finding derivatives is using the *USAF Stability and Control Datcom* (4) to check accuracy of calculation for important derivatives. The *Datcom* is a massive 3000 page report on finding stability and control derivatives created in 1975. It is most likely the source of many stability and control textbooks and provides the most information for derivative calculation. The derivatives are finally compared to those of the *Gossamer* aircraft because of the clear similarities between the three HPAs. The comparison between HPA derivatives will serve as an error checking method for derivative calculations.

Longitudinal Derivatives

There are 15 longitudinal derivatives associated with aircraft motion. These derivatives are important when determining the center of gravity location of the aircraft as well as determining elevator deflections and pitch stability. The longitudinal derivatives for the HPA are calculated and estimated using the equations shown in Table B-1. These equations are mostly from Etkin (3), but include some assumptions for simplicity. It is difficult to estimate these derivatives because of apparent mass effects that can only be found through flight testing (5).

Therefore, some of these derivatives are going to have an error. Table 4-1 gives all of the estimated longitudinal derivatives for the *Zephyrus*. Figure 4-1 shows a list of available longitudinal derivatives for the *Gossamer* aircraft. The values of the *Zephyrus* and *Gossamer* derivatives are on the same order of magnitude and compare well to each other.

Table 4-1. *Zephyrus* Longitudinal Derivatives

d_i/d_j	X	Z	M
Speed (U)	$C_{Xu} = -0.0266$	$C_{Zu} = 0$	$C_{Mu} = 0$
Angle of Attack (α)	$C_{X\alpha} = 0.2514$	$C_{Z\alpha} = -6.0210$	$C_{M\alpha} = -0.1203$
Pitch Rate (Q)	$C_{Xq} = 0$	$C_{Zq} = -4.3399$	$C_{Mq} = -28.3831$
Angle of Attack Rate (α dot)	$C_{X\alpha,dot} = 0$	$C_{Z\alpha,dot} = -0.6076$	$C_{M\alpha,dot} = -3.9736$
Elevator (δ_e)	$C_{X\delta_e} = 0$	$C_{Z\delta_e} = -0.3318$	$C_{M\delta_e} = -2.1699$

Item	Units	Condor (1977)	Albatross II (1980)	
			Standard Condition	High Speed
A. Trim Conditions				
Altitude	ft	sea level	sea level	sea level
Airspeed	ft/s (m/s)	16 (4.9)	20 (6.1)	28 (8.5)
Dynamic Pressure	lb/ft^2 (N/m^2)	.304 (14.6)	.476 (22.9)	.932 (44.8)
Lift	lb (N)	212 (944)	222 (988)	222 (988)
Drag	lb (N)	9.7 (43)	8.0 (36)	9.1 (41)
Lift/Drag	--	22	28	24
Static Margin	$\Delta Xac/\bar{c}$	-.045	-.16	+.002
Maneuver Margin	$\Delta Xmc/\bar{c}$	4.95	--	--
B. Longitudinal Derivatives (Out of Ground Effect)				
C_L	--	1.00	0.96	0.49
C_{L_α}	1/rad	5.40	5.58	6.15
$C_{L_{\dot{\alpha}}}$ (apparent mass)	1/rad	3.38	3.35	3.35
C_D	--	.0452	.0344	.0201
C_{D_α}	1/rad	0.061	0.045	0.021
C_{m_α}	1/rad	0.240	0.170	-0.010
C_{m_q}	1/rad	-10.0	-18.08	-18.20
$C_{m_{\dot{\alpha}}}$ (apparent mass)	1/rad	-.85	.23	.23
$C_{L_{\delta e}}$ (canard elevator)	1/rad	.66	.42	.42
$C_{D_{\delta e}}$ (canard elevator)	1/rad	0	.010	.003
$C_{m_{\delta e}}$ (canard elevator)	1/rad	1.26	1.84	1.84
$\partial T/\partial u$ (at .3 horsepower)	lb/ft/s (N/m/s)	-.60 (-8.8)	-.40 (-5.9)	-.32 (-4.7)
$\partial T/\partial hp$	lb/hp (N/W)	43 (.257)	22 (.131)	15.7 (.094)

Figure 4-1. Longitudinal Derivatives for the *Gossamer* Aircraft. This table is from the Appendix of the NASA stability and control analysis of the *Gossamer* aircraft (5).

Lateral Derivatives

There are also 15 lateral derivatives that define aircraft motion. These derivatives are very important to the study presented herein. They will define the lateral stability characteristics of the *Zephyrus* and must therefore be as accurate as possible. These derivatives will be used in the trimmed turn equations later on that define the aircraft's maneuverability. To ensure accuracy, equations from references 3, 6, and 7 will be used in determining the derivatives.

There are five derivatives that characterize each of the three lateral forces or moments on the aircraft. These forces and moments are differentiated with respect to side slip (β), roll rate (p), yaw rate (r), aileron input (δ_a), and rudder input (δ_r). There are no ailerons on the *Zephyrus*, so those derivatives are automatically zero. The derivatives with respect to β and r are most important because the *Zephyrus* must use β and r to control rolling moments on the aircraft as well as remain in a coordinated turn. The roll derivatives are all particularly important because they will determine the roll properties of the aircraft which are unique compared to any other aircraft. In particular the roll derivative with respect to yaw rate will have a huge effect on the aircraft's ability to trim at large banks. This is because the large lift differential between the faster moving outboard wing and slower moving inboard wing at low speeds creates a large rolling moment inward. The C_{Lr} derivative describes this motion.

The most difficult task in calculating the lateral derivatives is estimating values for the sidewash derivatives: $\partial\sigma/\partial\beta$, $\partial\sigma/\partial p$, and $\partial\sigma/\partial r$. Morelli, in reference to sidewash, states that "no data applicable to sailplanes are available at all (7)." Even the *USAF Stability and Control Datcom* only contains empirical estimation methods that are limited in application to higher speed aircraft (4). The best way to estimate these derivatives is by using the example stability and control properties of a sailplane to back calculate the derivatives. This is done for $\partial\sigma/\partial\beta$ using

sailplane data in Morelli (7). The $\partial\sigma/\partial p$ and $\partial\sigma/\partial r$ derivatives are not used because they are not given in Morelli's data.

Looking ahead to Equation (24), the roll moment on the aircraft in turn is determined by contributions from yaw rate, rudder deflection, and side slip. The contribution from the rudder deflection to roll is practically negligible. Therefore, the only thing keeping the aircraft from rolling inward in a turn is the side slip roll derivative $C_{L\beta}$. It is imperative that $C_{L\beta}$ be as accurate as possible to best determine the roll stability of the *Zephyrus*. The major contribution to $C_{L\beta}$ is the dihedral angle Γ. This angle is normally found by simple geometry. However, the nonlinearity of the *Zephyrus* wing makes finding Γ more challenging. The effective dihedral angle is calculated by breaking the wing into three panels and using a method by Beron-Rawdon (2). The dihedral is summed as a function of the moment fraction (MF) along the span for an elliptical lift distribution and the local dihedral angle for each respective panel (Equation 21).

$$\Gamma = \sum \Gamma_{local}(MF_{in} - MF_{out}) \tag{21}$$

The final lateral derivatives for the *Zephyrus* are given in Table 4-2. These are found using the equations in Table 4-3. These equations are a combination of equations from Etkin (3), McCormick (6), and Morelli (7). The complex lateral dynamics have made this process difficult, but the values displayed are the best possible estimation of derivatives given the available information. Comparison to the Gossamer derivatives in Figure 4-2 shows that a similar order of magnitude is observed between the derivatives. This helps validate the lateral derivatives for use in further stability calculations.

Table 4-2. *Zephyrus* Lateral Non-dimensional Derivatives

d_i/d_j	Y	L	N
Sideslip (β)	$C_{Y\beta} = -0.3462$	$C_{L\beta} = -0.3284$	$C_{N\beta} = 0.0797$
Roll Rate (P)	$C_{Yp} = -0.0150$	$C_{Lp} = -0.6979$	$C_{Np} = -0.0917$
Yaw Rate (R)	$C_{Yr} = 0.1922$	$C_{Lr} = 0.1902$	$C_{Nr} = -0.0443$
Aileron (δ_a)	$C_{Y\delta_a} = 0$	$C_{L\delta_a} = 0$	$C_{N\delta_a} = 0$
Rudder (δ_r)	$C_{Y\delta_r} = 0.4171$	$C_{L\delta_r} = 0.0075$	$C_{N\delta_r} = -0.0961$

Table 4-3. Lateral Non-dimensional Derivative Calculation

Y	L	N
$C_{Y\beta} = -a_{VT}\frac{S_{VT}}{S}(1-\frac{\partial\sigma}{\partial\beta})$	$C_{L\beta} = -\frac{a_{wb}}{6}\frac{(1+2\lambda)}{(1+\lambda)}\Gamma$	$C_{N\beta} = a_{VT}V_V(1-\frac{\partial\sigma}{\partial\beta})$
$C_{Yp} = -a_{VT}\frac{S_{VT}}{S}(\frac{2z_{VT}}{b})$	$C_{Lp} = -\frac{a_{wb}}{12}\frac{(1+3\lambda)}{(1+\lambda)}$	$C_{Np} = \frac{-C_{L0}}{12}\frac{(1+3\lambda)}{(1+\lambda)} + a_{VT}V_V\left(\frac{2z_{VT}}{b}\right)$
$C_{Yr} = a_{VT}\frac{S_{VT}}{S}(\frac{2l_{VT}}{b})$	$C_{Lr} = \frac{C_{L0}}{6}\frac{(1+3\lambda)}{(1+\lambda)}$	$C_{Nr} = -a_{VT}V_V(\frac{2l_{VT}}{b})$
$C_{Y\delta_a} = 0$	$C_{L\delta_a} = 0$	$C_{N\delta_a} = 0$
$C_{Y\delta_r} = a_{VT}\frac{S_{VT}}{S}$	$C_{L\delta_r} = a_{VT}\frac{S_{VT}z_{VT}}{Sb}$	$C_{N\delta_r} = -a_{VT}V_V$

Item	Units	Condor (1977)	Albatross II (1980)	
			Standard Condition	High Speed
C. Lateral Directional Derivatives (Body - Fixed Stability Axis System)				
C_{y_β}	1/rad	-.28	-.28	-.28
C_{ℓ_β}	1/rad	-.104	-.145	-.124
C_{ℓ_p}	1/rad	-.56	-.55	-.61
C_{ℓ_r}	1/rad	.250	.164	.122
C_{n_β}	1/rad	-.0050	.0079	.0022
C_{n_p}	1/rad	-.080	-.089	-.047
C_{n_r}	1/rad	-.0150	-.0048	-.0048
$C_{y_{\delta w}}$ (per side)	1/rad	0	0	0
$C_{\ell_{\delta w}}$ (per side)	1/rad	.56	.55	.61
$C_{n_{\delta w}}$ (per side)	1/rad	-.080	-.089	-.047
$C_{y_{\delta r}}$	1/rad	.083	.065	.022
$C_{\ell_{\delta r}}$	1/rad	0	0	0
$C_{n_{\delta r}}$	1/rad	.0340	.0152	.0052

Figure 4-2. Lateral Derivatives for the *Gossamer* Aircraft. This table is from the Appendix of the NASA stability and control analysis of the *Gossamer* aircraft (4).

Discussion of Longitudinal Static Stability

The simple estimation of these derivatives is acceptable because the aircraft has little risk of being pitch unstable. In fact, even if the derivatives provided evidence that the *Zephyrus* were unstable in pitch, the large pitch damping due to apparent mass effects (common among HPAs)

would make it relatively easy for the pilot to control minor instabilities. The Gossamer aircraft have a negative static margin and are longitudinally unstable (5). However, the large damping compensates for the static instability. This is why there is not a focus of longitudinal analysis in this thesis. Instead, the derivatives of the *Zephyrus* are just listed in Table 4-1 as a reference. The best use of longitudinal stability properties is to help determine the C.G. location using static margin. Equation (22) gives the C.G. location as a function of static stability margin for the *Zephyrus*. This equation can be used when weighting the aircraft to get a statically stable C.G. location before flight testing.

$$h = h_n - K_n \tag{22}$$

Analysis of Lateral Static Stability

The lateral stability properties of the *Zephyrus* are critical to proving that the mission is feasible. With the non-dimensional derivatives given in Table 4-2, a static trimmed turned solution is applied to find the side slip, rudder deflection, and yaw rate for a given bank angle. This is a dimensional analysis, so the derivatives from Table 4-2 are converted to dimensional derivatives using Table B-2. The relationships that describe lateral motion are given in Equations (23) through (25) which yield three unknowns: $\beta, \delta_r,$ and r. An important change is made to the $C_{L\beta}$ derivative in this analysis to account for aero-elastic effects of the wing. Equation (26) reflects an increase in wing dihedral angle due to the proportional increase in lift during a turn.

$$L = L_v \beta V + L_{\delta_r} \delta_r + L_r r = 0 \tag{23}$$

$$N = N_v \beta V + N_{\delta_r} \delta_r + N_r r = 0 \tag{24}$$

$$Y = Y_v \beta V + Y_{\delta_r} \delta_r + Y_r r = -W \sin(\phi) + mrV \tag{25}$$

$$C_{L\beta} = -(\frac{a_{wb}}{6}\frac{(1+2\lambda)}{(1+\lambda)}\Gamma)/\cos(\phi) \quad (26)$$

The equations above are solved in matrix form to give the trim solution for varying bank angle. The plots of each variable vs. bank angle are given in Figures 4-3 through 4-4. Figure 4-3 is the most important plot because side slip values will determine whether or not a trim solution is valid. Figure 4-3 shows that beta increases at roughly half the rate of bank angle. This is a marginally good solution. Side slip angles above 10º are an indication that the aircraft is difficult to trim. Figure 4-3 provides evidence that side slip will not surpass 8º when constrained to 15º banks. This is excellent analytical proof that 15º banked turns are possible in this aircraft.

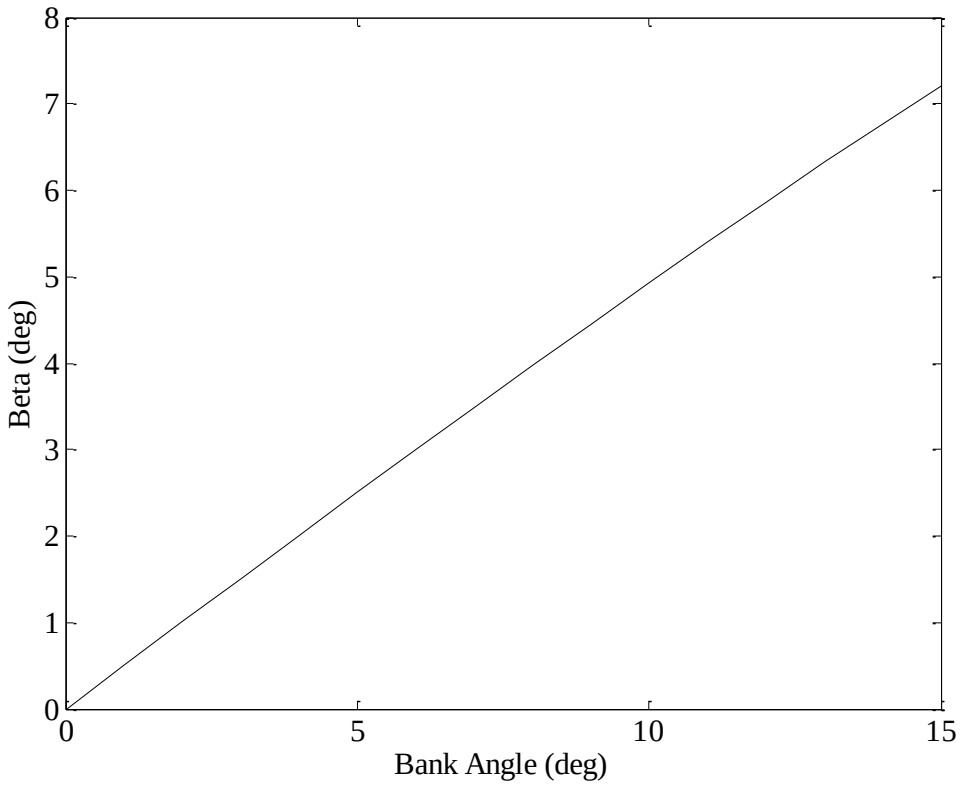

Figure 4-3. Side Slip vs. Bank Angle. This plot gives the linear relationship of side slip required to trim at a given bank angle turn.

An interesting result is observed in Figure 4-4. The rudder deflection required to turn is very small and is not linear when plotted against bank angle. This non-linearity is caused by the

aero-elastic effect in $C_{L\beta}$. Typically, an aircraft is considered spirally unstable if positive rudder deflection is required to trim in turn. However, the *Zephyrus* is floating right at zero rudder deflection and is therefore almost exactly marginally spirally stable in turn. This has occurred completely by chance, but will allow the pilot of the *Zephyrus* to easily control the aircraft in banked turns because rudder correction is not required to trim.

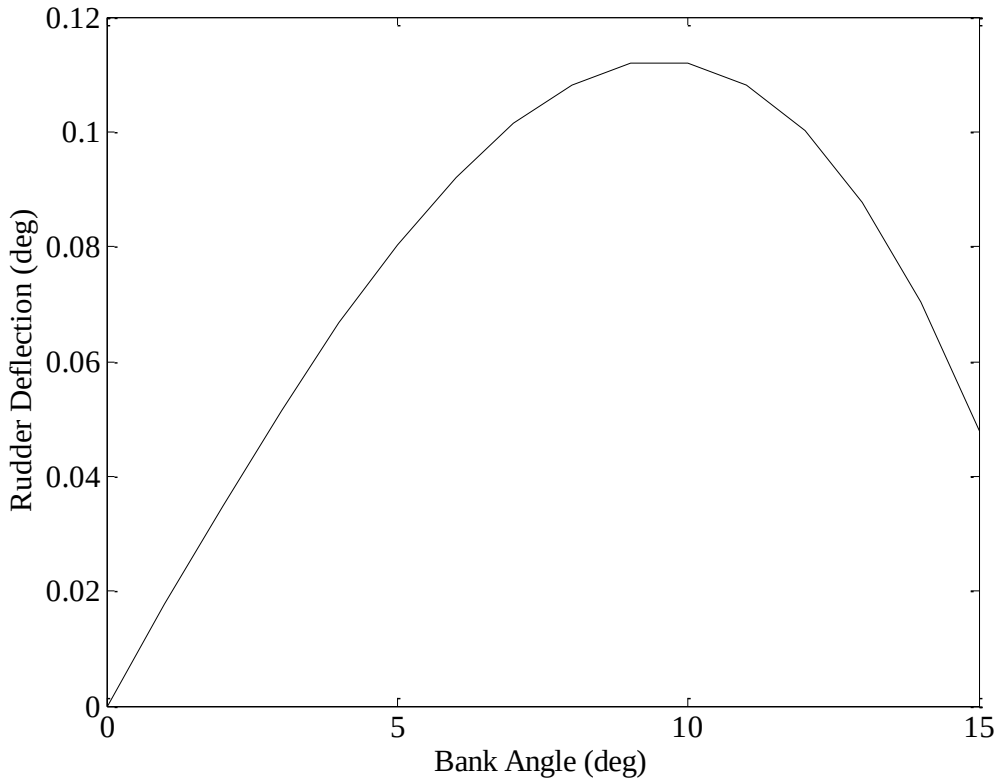

Figure 4-4. Rudder Deflection vs. Bank Angle. This plot gives the non-linear relationship of rudder deflection required to trim at a given bank angle turn. The plot indicates marginal spiral stability.

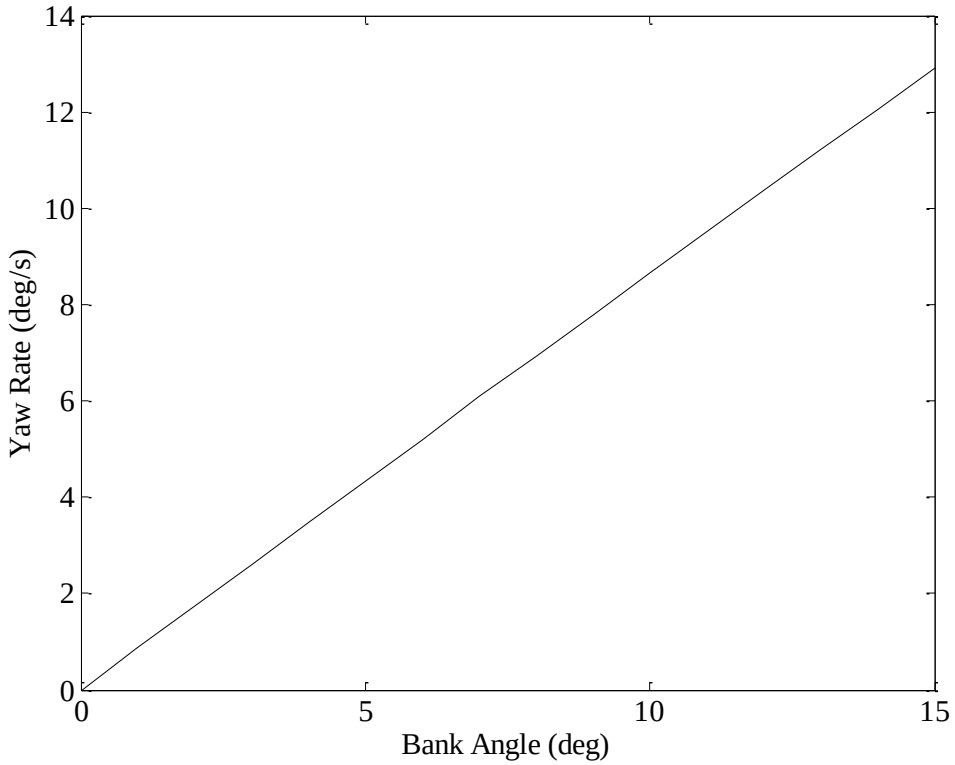

Figure 4-5. Yaw Rate vs. Bank Angle. This plot gives the linear relationship of yaw rate required to trim at a given bank angle turn.

The lateral stability analysis given in this thesis is a best estimate of the lateral characteristics of this aircraft. The estimate shows that the aircraft is suitable for lightly banked turns at side slip angles of up to 7º. This result is encouraging for the pursuit of the Kremer Prize, but it is not absolute. As stated in Jex's report, "roll and turn control is a major problem for human-powered aircraft (5)." Not only is it difficult to perform in flight, but it is difficult to predict by analysis. The lateral static stability of this aircraft will not be fully confirmed until a flight test takes place.

Discussion of Dynamic Stability Characteristics

It is difficult and somewhat arbitrary to attempt an analysis of the dynamic response of the *Zephyrus*. The dynamics of HPAs are very much dominated by nonlinearities due to aero-elasticity and apparent mass effects (5). These are very hard to simulate in analysis and are even more difficult to estimate for this particular aircraft. It's much more useful to discuss the potential dynamic response of the aircraft based on knowledge gained from Jex's report on the stability and control of the *Gossamer* aircraft. Concerning pitch dynamics, the dynamics of HPAs are very different from the second order modes characterized by most aircraft. The HPAs are characterized by first order modes that are dominated by large apparent mass and inertia terms. These first order instabilities have very large lag times and make the aircraft relatively easy to control in pitch (5).

The lateral dynamics of HPAs are much more complex. It is even tough to compare the lateral dynamics of the *Zephyrus* to the *Gossamer* aircraft because of the difference of control surfaces on the aircraft. However, the general conclusion can be made that yaw rates and roll rates are both characterized once again by significant lag times (5). This means that any instability would be relatively easy to control given that the control inputs have the necessary controlling effect. The only way to control roll in the *Zephyrus* is by inducing a sideslip that rolls the aircraft due to dihedral effects. There is a small possibility that any side slip will be a lagged reaction to rudder input and could potentially be too late to correct a hazardous flight condition. However, the dynamic complexities are very difficult to predict analytically. Gentle and precise flight testing is the best option for confirming lateral dynamic capabilities of the aircraft.

Chapter 5

Conclusion and Future Work

The work presented within has ranged a large category of performance analyses for the *Zephyrus*. Each of these analyses is attempting to answer one question: Can the *Zephyrus* win the Kremer prize? A performance analysis used a drag build-up to give the cruising airspeed range for the aircraft. An analysis of the course using a time integration MATLAB simulation then gave the course completion times for any given flight conditions. The time simulation also provided a constraint for the lateral control capabilities of the aircraft. Finally, stability characteristics that govern longitudinal and lateral aircraft motion were derived and calculated using a variety of methods and text references. These estimated characteristics provided the opportunity to perform a static stability analysis of the trimmed turn case for the aircraft. The final results of the turn solution gave the last part of an analytical answer to the aforementioned question of the aircraft's ability to win.

The answer to the question is yes. In the case of using 15º bank angle turns, the aircraft can complete the course with 30 seconds of time to spare at conservative wind conditions if flown at a cruise speed of 22 knots. This cruise speed is well within the performance power range of the aircraft. The bank angle analytically yields a large sideslip angle of 7º, but still yields a mission completion time that is safely within the limit. The side slip angles given in the trimmed turn solution are slightly higher than anticipated and could potentially limit performance. The performance drop would be caused by pressure drag from flow separation off of the fuselage pod. However, that the exact amount of increased drag due to side slip is not known. There is only one way to truly get an absolute idea of the capabilities of the aircraft. A flight test has been planned

for the end of the spring 2013 semester that will test the limits defined in this analysis. The data provided gives analytical meaning to flight testing objectives. The flight testing coupled with the analysis herein will be a huge landmark for the *Zephyrus* project in safety and mission feasibility and is the final step before officially competing for the Kremer Prize.

The direct applications of a human powered aircraft to the current aerospace industry are clearly limited by the aircraft's lack of practical use. However, the design and fabrication of a human powered aircraft provides a significant learning opportunity to aerospace students and presents unique challenges in design and analysis as expressed in this thesis. The amount of leadership, teamwork, and problem solving experience that students receive working on an HPA project is extremely valuable to industry in an indirect way. The *Zephyrus* has provided many grateful undergraduates at Penn State the opportunity to think critically about aerospace engineering as displayed in this thesis.

Appendix A

MATLAB Files

Time Simulation and Turn Plotting Script

Note that this particular MATLAB script was converted from a script to a function for use in the time data gathering and contour plotting script. The only difference between this script and that function are the removal of plotting code and addition of function related code notation.

```
%Flight Path Time Simulation and Turn Plotting
%Peter Blasco
%4/1/13

clear
clc
close all

g=9.81;  %m/s^2
length=0;

%Inputs
Vh=input('Please enter cruise speed (kts): ');
Vh=Vh*(1/1.943844);
bank=input('Please enter bank angle (deg): ');
Vw=input('Please enter wind speed (m/s): ');

%Clockwise Lap
%Solve for turn radius, angular velocity of turn, and time period
r=(Vh^2)/(g*tan(bank*(pi/180)));
CC=2*pi*r;
w=Vh/r;
T=(2*pi)/w;
%Round T for use in loop iterations
TR=round(((2*pi)/w)*100)/100;

%Set time increment and array
dt=0.01;
t=0:dt:TR;

%Solve for Vx and Vy at each time based on theta
theta=w.*t;
Vy=Vh.*cos(theta)-Vw;
Vx=Vh.*sin(theta);
```

```
VCy=Vh.*cos(theta);
VCx=Vh.*sin(theta);

%Initialize x and y
x=zeros(1,(TR/dt)+1);
y=zeros(1,(TR/dt)+1);
Cx=zeros(1,(TR/dt)+1);
Cy=zeros(1,(TR/dt)+1);

%Loop increments x and y by changes in vx and vy times dt
for i=1:(TR/dt)

    Cx(i+1)=Cx(i)+VCx(i)*dt;
    Cy(i+1)=Cy(i)+VCy(i)*dt;
    x(i+1)=x(i)+Vx(i)*dt;
    y(i+1)=y(i)+Vy(i)*dt;
    length=length+sqrt((x(i+1)-x(i))^2+(y(i+1)-y(i))^2);

end

%Solve for V23 and angles
a23=1+(tan(deg2rad(30)))^2;
b23=-2*Vw*tan(deg2rad(30));
c23=Vw^2-Vh^2;

Vx23=(-b23+sqrt(b23^2-(4*a23*c23)))/(2*a23);

Vhy23=sqrt(Vh^2-Vx23^2);
Vy23=Vhy23+Vw;
V23=sqrt(Vx23^2+Vy23^2);

theta1=acos(Vx23/Vh)+pi/2;
theta2=(2*pi)-(2*theta1);
theta3=theta1;

tt1=theta1/w;
tt2=theta2/w;
tt3=theta3/w;

%Estimate straight leg distances
d1=500;
d2=500-((length-CC)/2);
d3=d2;

%Calculate time to traverse straight legs
t1=d1/(Vh-Vw);
t2=d2/(V23);
t3=t2;

Ttot1=t1+t2+t3+tt1+tt2+tt3;
```

```
%Counter-clockwise Lap

a46=1+(tan(deg2rad(30)))^2;
b46=2*Vw*tan(deg2rad(30));
c46=Vw^2-Vh^2;

Vx46=(-b46+sqrt(b46^2-(4*a46*c46)))/(2*a46);

Vhy46=sqrt(Vh^2-Vx46^2);
Vy46=Vhy46-Vw;
V46=sqrt(Vx46^2+Vy46^2);

theta4=acos(Vx46/Vh)+pi/2;
theta5=theta4;

tt4=theta4/w;
tt5=theta5/w;

d4=520;
d5=500-(length-CC);
d6=d4;

t4=d4/(V46);
t5=d5/(Vh+Vw);
t6=t4;

Ttot2=t4+t5+t6+tt4+tt5;

Ttot=Ttot1+Ttot2;

%Plots x vs. y giving a 2D ground track of the aircraft
index1=round(theta1*100/w);
index2=round(theta2*100/w)+index1;
index3=round(theta3*100/w)+index2;
index4=round((pi-theta4)*100/w);
index5=round(pi*100/w);
index6=round(theta4*100/w)+index5;

subplot(2,3,1);
plot(x(1:index1),y(1:index1),'k');
title(sprintf('Turn One at %1.1f m/s Wind',Vw));
axis equal;
xlabel('x (m)');
ylabel('y (m)');
legend(sprintf('Bank Angle = %1.1f deg',bank),'location','south');

subplot(2,3,2);
plot(x(index1:index2),y(index1:index2),'k');
title(sprintf('Turn Two at %1.1f m/s Wind',Vw));
axis equal;
xlabel('x (m)');
ylabel('y (m)');
```

```
legend(sprintf('Bank Angle = %1.1f deg',bank),'location','west');

subplot(2,3,3);
plot(x(index2:index3),y(index2:index3),'k');
title(sprintf('Turn Three at %1.1f m/s Wind',Vw));
axis equal;
xlabel('x (m)');
ylabel('y (m)');
legend(sprintf('Bank Angle = %1.1f deg',bank),'location','south');

subplot(2,3,4);
plot(-x(index4:index5),y(index4:index5),'k');
title(sprintf('Turn Four at %1.1f m/s Wind',Vw));
axis equal;
xlabel('x (m)');
ylabel('y (m)');
legend(sprintf('Bank Angle = %1.1f deg',bank),'location','southeast');

subplot(2,3,5);
plot(-x(index5:index6),y(index5:index6),'k');
title(sprintf('Turn Five at %1.1f m/s Wind',Vw));
axis equal;
xlabel('x (m)');
ylabel('y (m)');
legend(sprintf('Bank Angle = %1.1f deg',bank),'location','northeast');

%Info
disp(' ');
disp('Lap One');
fprintf('Time to complete leg 1 = %1.1f s \n',t1/2);
fprintf('Time to complete turn 1 = %1.1f s \n',tt1);
fprintf('Time to complete leg 2 = %1.1f s \n',t2);
fprintf('Time to complete turn 2 = %1.1f s \n',tt2);
fprintf('Time to complete leg 3 = %1.1f s \n',t3);
fprintf('Time to complete turn 3 = %1.1f s \n',tt3);
fprintf('Time to complete leg 4 = %1.1f s \n',t1/2);
disp(' ');
disp('Lap Two');
fprintf('Time to complete leg 5 = %1.1f s \n',t4);
fprintf('Time to complete turn 4 = %1.1f s \n',tt4);
fprintf('Time to complete leg 6 = %1.1f s \n',t5);
fprintf('Time to complete turn 5 = %1.1f s \n',tt5);
fprintf('Time to complete leg 7 = %1.1f s \n',t6);
disp(' ');
fprintf('Time to complete lap one = %1.1f s \n',Ttot1);
fprintf('Time to complete lap two = %1.1f s \n',Ttot2);
fprintf('Time to complete course = %1.1f s \n',Ttot);
fprintf('Spare time = %1.1f s \n',420-Ttot);

figure
plot(x,y,Cx,Cy);
axis equal;
```

Time Data Collection and Contour Plotting Script

```
%Data Gathering for HPA Time Simulation
%Peter Blasco
%4/1/13

clear
clc
close all

%Wind Speed and Airspeed
n=50;
Vh=19.5:(24-19.5)/n:24;

bank=5:(30-5)/n:30;
Vw=6;

REC=zeros(n+1,n+1);
trem=zeros(n+1,n+1);
for i=1:n+1
    for k=1:n+1
        [Ttotal,trm]=timesim(Vh(i),bank(k),Vw);
        REC(i,k)=Ttotal;
        trem(i,k)=trm;
    end
end

contourf(bank,Vh,REC);
title('Analyzing Bank Angle and Airspeed');
xlabel('Bank Angle (deg)');
ylabel('Cruise Airspeed (kts)');
colorbar;
hold off

%Bank Angle and Airspeed
bank=15;
Vw=5:(7-5)/n:7;


for i=1:n+1
    for k=1:n+1
        [Ttotal,trm]=timesim(Vh(i),bank,Vw(k));
        REC(i,k)=Ttotal;
        trem(i,k)=trm;
    end
end

%Plot contour plots to give visual representation of data
figure
hold on
contourf(Vw*1.9438,Vh,REC);
title('Analyzing Bank Angle and Airspeed');
```

```
xlabel('Wind Speed (kts)');
ylabel('Cruise Airspeed (kts)');
colorbar;
```

Zephyrus Stability Parameters and Linear Model Script

Note that this particular MATLAB script was converted from a script to a function for use in the bank angle vs. trim turn solution variables plotting script (the script given). The only difference between this script and that function are the removal of plotting code and addition of function related code notation.

```
%Zephyrus Stability and Control Code
%Peter Blasco        4/8/2013
clear
clc
close all
%Parameters

V=37;           %ft/s
p=0.002377;  %slugs/ft^3

W=208;        %lbs
g=32.2;
m=W/g;
b=73.8;       %ft
S=163.7;      %ft^2
taper=0.302;
AR=b^2/S;
Sht=12.64;
Svt=15.89;
c=2.37;       %ft
cht=1.47;
hnwb=0.17;    %guess
at=4.297;     %/rad
avt=4.297;
ae=at;
ar=avt;
awb=5.73;
lt=15.5;
lf=17;
zf=1.33;
eo=0;
dedal=0.14;
it=0;
Cmacwb=-.05; %guess
Cmop=0;
Cmpal=0;
```

```
a=awb*(1+((at*Sht)/(awb*S))*(1-dedal));
Vh=(Sht*lt)/(S*c);
Vv=(Svt*lf)/(S*b);
Kn=0.02;     %guess
Cdo=0.0133;   %From Drag Buildup
eos=0.82;
dodbeta=0.17;
dihed= 16.01*(pi/180);    %rad

%Longitudinal Static Stability
hn=hnwb+((at/a)*Vh*(1-dedal));
%Clde=ae*(Sht/S);
%Cmde=(Clde.*(hn-Kn-hnwb))-(Vh*ae);
Cmal=a.*-Kn;
Cmo=Cmacwb+Cmop+(at*Vh*(eo+it)*(1-((at*Sht)/(a*S))*(1-dedal)));

Clo=(2*W)/(p*V^2*S);
alpha0=-4*(pi/180);

%Non-dimensional Derivatives - Longitudinal
Cxu=-2*Cdo;
Cxal=Clo+(a*alpha0)-((2*a*Clo)/(pi*eos*AR));
Cxq=0;
Cxaldot=0;
Cxde=0;
Czu=0;
Czal=-a-Cdo-((2*Clo*a*alpha0)/(pi*eos*AR));
Czq=-2*at*Vh;
Czaldot=-2*at*Vh*dedal;
Czde=-ae*(Sht/S);
Cmu=0;
%Already have Cmal
Cmq=-2*at*Vh*(lt/c);
Cmaldot=-2*at*Vh*(lt/c)*dedal;
Cmde=-ae*Vh;

%Lateral Static Stability

%Non-dimensional Derivatives - Lateral

Cyb=-avt*Svt/S*(1-dodbeta);
Cyp=-avt*Svt/S*((2*zf/b));
Cyr=avt*Svt/S*((2*lf/b));
Cyda=0;
Cydr=ar*(Svt/S);
Clb=-(awb/6)*((1+2*taper)/(1+taper))*dihed;
Clp=-(awb/12)*((1+3*taper)/(1+taper));
Clr=(Clo/6)*((1+3*taper)/(1+taper));
Clda=0;
Cldr=ar*((Svt*zf)/(S*b));
Cnb=avt*Vv*(1-dodbeta);
Cnp=-(Clo/12)*((1+3*taper)/(1+taper))+avt*Vv*((2*zf/b));
Cnr=-avt*Vv*((2*lf/b));
Cnda=0;
```

```
Cndr=-ar*Vv;

%Dimensional Stability
uo=V;
Cwo=Clo;
thetao=0;

%Longitudinal Dimensional Derivatives
Xu=p*uo*S*Cwo*sin(thetao)+0.5*p*uo*S*Cxu;
Xw=0.5*p*uo*S*Cxal;
Xq=0.25*p*uo*c*S*Cxq;
Xwdot=0.25*p*c*S*Cxaldot;
Xde=0.5*p*uo^2*S*Cxde;
Zu=-p*uo*S*Cwo*cos(thetao)+0.5*p*uo*S*Czu;
Zw=0.5*p*uo*S*Czal;
Zq=0.25*p*uo*c*S*Czq;
Zwdot=0.25*p*c*S*Czaldot;
Zde=0.25*p*uo^2*S*Czde;
Mu=0.5*p*uo*c*S*Cmu;
Mw=0.5*p*uo*c*S*Cmal;
Mq=0.25*p*uo*c^2*S*Cmq;
Mwdot=0.25*p*c^2*S*Cmaldot;
Mde=0.5*p*uo^2*c*S*Cmde;

%Lateral Dimensional Derivatives
Yv=0.5*p*uo*S*Cyb;
Yp=0.25*p*uo*b*S*Cyp;
Yr=0.25*p*uo*b*S*Cyr;
Yda=0.5*p*uo^2*S*Cyda;
Ydr=0.5*p*uo^2*S*Cydr;
Lv=0.5*p*uo*b*S*Clb;
Lp=0.25*p*uo*b^2*S*Clp;
Lr=0.25*p*uo*b^2*S*Clr;
Lda=0.5*p*uo^2*b*S*Clda;
Ldr=0.5*p*uo^2*b*S*Cldr;
Nv=0.5*p*uo*b*S*Cnb;
Np=0.25*p*uo*b^2*S*Cnp;
Nr=0.25*p*uo*b^2*S*Cnr;
Nda=0.5*p*uo^2*b*S*Cnda;
Ndr=0.5*p*uo^2*b*S*Cndr;


LOMAT=[Cxu Czu Cmu;Cxal Czal Cmal;Cxq Czq Cmq;Cxaldot Czaldot
Cmaldot;Cxde Czde Cmde];
LAMAT=[Cyb Clb Cnb;Cyp Clp Cnp;Cyr Clr Cnr;Cyda Clda Cnda;Cydr Cldr
Cndr];
disp('Nondimensional Longitudinal Derivatives');
disp(LOMAT);
disp('Nondimensional Lateral Derivatives');
disp(LAMAT);

%Lateral Trim solution
bank=0:15;
recb=zeros(16);
```

```
recdr=zeros(16);
recr=zeros(16);
for i=1:16
    [b,dr,r]=turntrim(bank(i));
    recb(i)=b;
    recdr(i)=dr;
    recr(i)=r;
end

plot(bank,recb,'k');
xlabel('Bank Angle (deg)');
ylabel('Beta (deg)');

figure
plot(bank,recdr,'k');
xlabel('Bank Angle (deg)');
ylabel('Rudder Deflection (deg)');

figure
plot(bank,recr,'k');
xlabel('Bank Angle (deg)');
ylabel('Yaw Rate (deg/s)');
```

Ventus Turn Drag Script

```
%Ventus Drag for varying bank angles
clear
clc
close all

phi=0:15:60;
Delta=zeros(1,5);
for i=1:5
    [v,D,Dmin]=vendrag(phi(i));
    vrec(i,:)=v;
    Drec(i,:)=D;
    Dminrec(i,:)=Dmin;
end

for i=1:4
    Delta(i+1)=((Dminrec(i+1,:)-Dminrec(i,:))/Dminrec(i,:))*100;
end

plot(vrec(1,:),Drec(1,:),vrec(2,:),Drec(2,:),vrec(3,:),Drec(3,:),vrec(4
,:),Drec(4,:),vrec(5,:),Drec(5,:));
xlabel('Velocity');
ylabel('Drag');
legend('0','15','30','45','60');

figure
```

```
plot(0:15:60,Delta,'k');
xlabel('Bank Angle (deg)');
ylabel('Increase in Minimum Drag (%)');
```

Ventus Drag Calculation Function

```
function [v,D,Dmin] = vendrag(phi)

%Parameters
W=5880;      %N
S=11.03;     %m^2
b=18;        %m
Sin=2*2.424;  %m^2
Smid=2*2.64953;
Sout=2*0.3997;
Svt=1.126;
Sht=1.0306;
Swl=2*0.13;
cin=0.71;    %m
cmid=0.585;
cout=0.43;
cvt=0.9339;
cht=0.47;
cwl=0.1899;
p=1.225;     %kg/m^3
u=1.79e-5;   %m^2/s
e=1.05;
AR=b^2/S;
cnv=0.224808942443;   %convert Newtons to lbs
mtk=1.9438;    %converts m/s to kts

%Turn Parameters
phirad=phi*(pi/180);

%Fuselage geometry
h=[0.083 0.709 0.814 0.57 0.333 0.257 0.189];
w=[0.096 0.547 0.619 0.464 0.357 0.255 0.157];
a=w./2;
b=h./2;
P=pi.*(3.*(a+b)-((3.*a+b).*(a+3.*b)).^0.5);  %ramanujan
dx=1;
A=zeros(1,6);
for i=1:6
    A(i)=0.5*(P(i)+P(i+1))*dx;
end

%Velocity Constraints
vmin=27;
vmax=61;
dv=0.1;
```

```
%Drag Polars

DRAG POLARS NOT SHOWN

%Intialize all variables
n=((vmax-vmin)/dv);
Cdprofin1=zeros(1,n);
Cdprofin2=zeros(1,n);
Cdprofin=zeros(1,n);
Cdprofmid1=zeros(1,n);
Cdprofmid2=zeros(1,n);
Cdprofmid=zeros(1,n);
Cdprofout1=zeros(1,n);
Cdprofout2=zeros(1,n);
Cdprofout=zeros(1,n);
Cdprofwl1=zeros(1,n);
Cdprofwl2=zeros(1,n);
Cdprofwl=zeros(1,n);
Cdprofvt1=zeros(1,n);
Cdprofvt2=zeros(1,n);
Cdprofvt=zeros(1,n);
Cdprofht1=zeros(1,n);
Cdprofht2=zeros(1,n);
Cdprofht=zeros(1,n);
v=zeros(1,n);
Rein=zeros(1,n);
Remid=zeros(1,n);
Reout=zeros(1,n);
Rewl=zeros(1,n);
ReVT=zeros(1,n);
ReHT=zeros(1,n);
Cl=zeros(1,n);
Cdi=zeros(1,n);
Cdprof=zeros(1,n);
Cd=zeros(1,n);
Cdvt=zeros(1,n);
Cdht=zeros(1,n);
D=zeros(1,n);
Dw=zeros(1,n);
Dvt=zeros(1,n);
Dht=zeros(1,n);
Df=zeros(1,n);
Dint=zeros(1,n);
Dwp=zeros(1,n);
Dwi=zeros(1,n);
qS=zeros(1,n);
LD=zeros(1,n);
Rex=zeros(1,6);
Cfx=zeros(1,6);
Fj=zeros(1,6);
Vsink=zeros(1,n);

%Drag Calculating Loop
```

```
for i=1:n
    v(i)=(i-1)*dv+vmin;
    Rein(i)=(p*v(i)*cin)/u;
    Remid(i)=(p*v(i)*cmid)/u;
    Reout(i)=(p*v(i)*cout)/u;
    Rewl(i)=(p*v(i)*cwl)/u;
    ReVT(i)=(p*v(i)*cvt)/u;
    ReHT(i)=(p*v(i)*cht)/u;
    Rewl(i)=(p*v(i)*cwl)/u;
    Cl(i)=(2*W)/(p*S*v(i)^2*cos(phirad));

    %Profile Drag Coefficient of Inboard Wing Section
    if Rein(i)>=325000 && Rein(i)<700000
        Cdprofin1(i)=(Sin/S)*interp1(ClRe325In,CdRe325In,Cl(i));
        Cdprofin2(i)=(Sin/S)*interp1(ClRe700In,CdRe700In,Cl(i));
        Cdprofin(i)=(Cdprofin1(i)+Cdprofin2(i))/2;
    elseif Rein(i)>=700000 && Rein(i)<1000000
        Cdprofin1(i)=(Sin/S)*interp1(ClRe700In,CdRe700In,Cl(i));
        Cdprofin2(i)=(Sin/S)*interp1(ClRe1000In,CdRe1000In,Cl(i));
        Cdprofin(i)=(Cdprofin1(i)+Cdprofin2(i))/2;
    elseif Rein(i)>=1000000 && Rein(i)<1500000
        Cdprofin1(i)=(Sin/S)*interp1(ClRe1000In,CdRe1000In,Cl(i));
        Cdprofin2(i)=(Sin/S)*interp1(ClRe1500In,CdRe1500In,Cl(i));
        Cdprofin(i)=(Cdprofin1(i)+Cdprofin2(i))/2;
    elseif Rein(i)>=1500000 && Rein(i)<2000000
        Cdprofin1(i)=(Sin/S)*interp1(ClRe1500In,CdRe1500In,Cl(i));
        Cdprofin2(i)=(Sin/S)*interp1(ClRe2000In,CdRe2000In,Cl(i));
        Cdprofin(i)=(Cdprofin1(i)+Cdprofin2(i))/2;
    elseif Rein(i)>=2000000 && Rein(i)<3000000
        Cdprofin1(i)=(Sin/S)*interp1(ClRe2000In,CdRe2000In,Cl(i));
        Cdprofin2(i)=(Sin/S)*interp1(ClRe3000In,CdRe3000In,Cl(i));
        Cdprofin(i)=(Cdprofin1(i)+Cdprofin2(i))/2;
    elseif Rein(i)>=3000000 && Rein(i)<4000000
        Cdprofin1(i)=(Sin/S)*interp1(ClRe3000In,CdRe3000In,Cl(i));
        Cdprofin2(i)=(Sin/S)*interp1(ClRe4000In,CdRe4000In,Cl(i));
        Cdprofin(i)=(Cdprofin1(i)+Cdprofin2(i))/2;
    elseif Rein(i)>=4000000 && Rein(i)<6000000
        Cdprofin1(i)=(Sin/S)*interp1(ClRe4000In,CdRe4000In,Cl(i));
        Cdprofin2(i)=(Sin/S)*interp1(ClRe6000In,CdRe6000In,Cl(i));
        Cdprofin(i)=(Cdprofin1(i)+Cdprofin2(i))/2;
    end

    %Profile Drag Coefficient of Mid Wing Section
    if Remid(i)>=325000 && Remid(i)<700000
        Cdprofmid1(i)=(Smid/S)*interp1(ClRe325Mid,CdRe325Mid,Cl(i));
        Cdprofmid2(i)=(Smid/S)*interp1(ClRe700Mid,CdRe700Mid,Cl(i));
        Cdprofmid(i)=(Cdprofmid1(i)+Cdprofmid2(i))/2;
    elseif Remid(i)>=700000 && Remid(i)<1000000
        Cdprofmid1(i)=(Smid/S)*interp1(ClRe700Mid,CdRe700Mid,Cl(i));
        Cdprofmid2(i)=(Smid/S)*interp1(ClRe1000Mid,CdRe1000Mid,Cl(i));
        Cdprofmid(i)=(Cdprofmid1(i)+Cdprofmid2(i))/2;
    elseif Remid(i)>=1000000 && Remid(i)<1500000
        Cdprofmid1(i)=(Smid/S)*interp1(ClRe1000Mid,CdRe1000Mid,Cl(i));
        Cdprofmid2(i)=(Smid/S)*interp1(ClRe1500Mid,CdRe1500Mid,Cl(i));
```

```
    Cdprofmid(i)=(Cdprofmid1(i)+Cdprofmid2(i))/2;
elseif Remid(i)>=1500000 && Remid(i)<2000000
    Cdprofmid1(i)=(Smid/S)*interp1(ClRe1500Mid,CdRe1500Mid,Cl(i));
    Cdprofmid2(i)=(Smid/S)*interp1(ClRe2000Mid,CdRe2000Mid,Cl(i));
    Cdprofmid(i)=(Cdprofmid1(i)+Cdprofmid2(i))/2;
elseif Remid(i)>=2000000 && Remid(i)<3000000
    Cdprofmid1(i)=(Smid/S)*interp1(ClRe2000Mid,CdRe2000Mid,Cl(i));
    Cdprofmid2(i)=(Smid/S)*interp1(ClRe3000Mid,CdRe3000Mid,Cl(i));
    Cdprofmid(i)=(Cdprofmid1(i)+Cdprofmid2(i))/2;
elseif Remid(i)>=3000000 && Remid(i)<4000000
    Cdprofmid1(i)=(Smid/S)*interp1(ClRe3000Mid,CdRe3000Mid,Cl(i));
    Cdprofmid2(i)=(Smid/S)*interp1(ClRe4000Mid,CdRe4000Mid,Cl(i));
    Cdprofmid(i)=(Cdprofmid1(i)+Cdprofmid2(i))/2;
elseif Remid(i)>=4000000 && Remid(i)<6000000
    Cdprofmid1(i)=(Smid/S)*interp1(ClRe4000Mid,CdRe4000Mid,Cl(i));
    Cdprofmid2(i)=(Smid/S)*interp1(ClRe6000Mid,CdRe6000Mid,Cl(i));
    Cdprofmid(i)=(Cdprofmid1(i)+Cdprofmid2(i))/2;
end

%Profile Drag Coefficient of Outer Wing Section
if Reout(i)>=325000 && Reout(i)<700000
    Cdprofout1(i)=(Sout/S)*interp1(ClRe325Out,CdRe325Out,Cl(i));
    Cdprofout2(i)=(Sout/S)*interp1(ClRe700Out,CdRe700Out,Cl(i));
    Cdprofout(i)=(Cdprofout1(i)+Cdprofout2(i))/2;
elseif Reout(i)>=700000 && Reout(i)<1000000
    Cdprofout1(i)=(Sout/S)*interp1(ClRe700Out,CdRe700Out,Cl(i));
    Cdprofout2(i)=(Sout/S)*interp1(ClRe1000Out,CdRe1000Out,Cl(i));
    Cdprofout(i)=(Cdprofout1(i)+Cdprofout2(i))/2;
elseif Reout(i)>=1000000 && Reout(i)<1500000
    Cdprofout1(i)=(Sout/S)*interp1(ClRe1000Out,CdRe1000Out,Cl(i));
    Cdprofout2(i)=(Sout/S)*interp1(ClRe1500Out,CdRe1500Out,Cl(i));
    Cdprofout(i)=(Cdprofout1(i)+Cdprofout2(i))/2;
elseif Reout(i)>=1500000 && Reout(i)<2000000
    Cdprofout1(i)=(Sout/S)*interp1(ClRe1500Out,CdRe1500Out,Cl(i));
    Cdprofout2(i)=(Sout/S)*interp1(ClRe2000Out,CdRe2000Out,Cl(i));
    Cdprofout(i)=(Cdprofout1(i)+Cdprofout2(i))/2;
elseif Reout(i)>=2000000 && Reout(i)<3000000
    Cdprofout1(i)=(Sout/S)*interp1(ClRe2000Out,CdRe2000Out,Cl(i));
    Cdprofout2(i)=(Sout/S)*interp1(ClRe3000Out,CdRe3000Out,Cl(i));
    Cdprofout(i)=(Cdprofout1(i)+Cdprofout2(i))/2;
elseif Reout(i)>=3000000 && Reout(i)<4000000
    Cdprofout1(i)=(Sout/S)*interp1(ClRe3000Out,CdRe3000Out,Cl(i));
    Cdprofout2(i)=(Sout/S)*interp1(ClRe4000Out,CdRe4000Out,Cl(i));
    Cdprofout(i)=(Cdprofout1(i)+Cdprofout2(i))/2;
elseif Reout(i)>=4000000 && Reout(i)<6000000
    Cdprofout1(i)=(Sout/S)*interp1(ClRe4000Out,CdRe4000Out,Cl(i));
    Cdprofout2(i)=(Sout/S)*interp1(ClRe6000Out,CdRe6000Out,Cl(i));
    Cdprofout(i)=(Cdprofout1(i)+Cdprofout2(i))/2;
end

%Profile Drag Coefficient of Winglet Section
if Rewl(i)>=35000 && Rewl(i)<45000
    Cdprofwl1(i)=(Swl/S)*interp1(ClRe35Wl,CdRe35Wl,Cl(i));
    Cdprofwl2(i)=(Swl/S)*interp1(ClRe45Wl,CdRe45Wl,Cl(i));
```

```
    Cdprofwl(i)=(Cdprofwl1(i)+Cdprofwl2(i))/2;
elseif Rewl(i)>=45000 && Rewl(i)<60000
    Cdprofwl1(i)=(Swl/S)*interp1(ClRe45Wl,CdRe45Wl,Cl(i));
    Cdprofwl2(i)=(Swl/S)*interp1(ClRe60Wl,CdRe60Wl,Cl(i));
    Cdprofwl(i)=(Cdprofwl1(i)+Cdprofwl2(i))/2;
elseif Rewl(i)>=60000 && Rewl(i)<100000
    Cdprofwl1(i)=(Swl/S)*interp1(ClRe60Wl,CdRe60Wl,Cl(i));
    Cdprofwl2(i)=(Swl/S)*interp1(ClRe100Wl,CdRe100Wl,Cl(i));
    Cdprofwl(i)=(Cdprofwl1(i)+Cdprofwl2(i))/2;
elseif Rewl(i)>=100000 && Rewl(i)<200000
    Cdprofwl1(i)=(Swl/S)*interp1(ClRe100Wl,CdRe100Wl,Cl(i));
    Cdprofwl2(i)=(Swl/S)*interp1(ClRe200Wl,CdRe200Wl,Cl(i));
    Cdprofwl(i)=(Cdprofwl1(i)+Cdprofwl2(i))/2;
elseif Rewl(i)>=200000 && Rewl(i)<400000
    Cdprofwl1(i)=(Swl/S)*interp1(ClRe200Wl,CdRe200Wl,Cl(i));
    Cdprofwl2(i)=(Swl/S)*interp1(ClRe400Wl,CdRe400Wl,Cl(i));
    Cdprofwl(i)=(Cdprofwl1(i)+Cdprofwl2(i))/2;
elseif Rewl(i)>=400000 && Rewl(i)<500000
    Cdprofwl1(i)=(Swl/S)*interp1(ClRe400Wl,CdRe400Wl,Cl(i));
    Cdprofwl2(i)=(Swl/S)*interp1(ClRe500Wl,CdRe500Wl,Cl(i));
    Cdprofwl(i)=(Cdprofwl1(i)+Cdprofwl2(i))/2;
elseif Rewl(i)>=500000 && Rewl(i)<700000
    Cdprofwl1(i)=(Swl/S)*interp1(ClRe500Wl,CdRe500Wl,Cl(i));
    Cdprofwl2(i)=(Swl/S)*interp1(ClRe700Wl,CdRe700Wl,Cl(i));
    Cdprofwl(i)=(Cdprofwl1(i)+Cdprofwl2(i))/2;
elseif Rewl(i)>=700000 && Rewl(i)<1000000
    Cdprofwl1(i)=(Swl/S)*interp1(ClRe700Wl,CdRe700Wl,Cl(i));
    Cdprofwl2(i)=(Swl/S)*interp1(ClRe1000Wl,CdRe1000Wl,Cl(i));
    Cdprofwl(i)=(Cdprofwl1(i)+Cdprofwl2(i))/2;
elseif Rewl(i)>=1000000 && Rewl(i)<1300000
    Cdprofwl1(i)=(Swl/S)*interp1(ClRe1000Wl,CdRe1000Wl,Cl(i));
    Cdprofwl2(i)=(Swl/S)*interp1(ClRe1300Wl,CdRe1300Wl,Cl(i));
    Cdprofwl(i)=(Cdprofwl1(i)+Cdprofwl2(i))/2;
elseif Rewl(i)>=1300000 && Rewl(i)<1600000
    Cdprofwl1(i)=(Swl/S)*interp1(ClRe1300Wl,CdRe1300Wl,Cl(i));
    Cdprofwl2(i)=(Swl/S)*interp1(ClRe1600Wl,CdRe1600Wl,Cl(i));
    Cdprofwl(i)=(Cdprofwl1(i)+Cdprofwl2(i))/2;
end

%Total Profile Drag for the Wing
Cdprof(i)=Cdprofin(i)+Cdprofmid(i)+Cdprofout(i)+Cdprofwl(i);
Dwp(i)=0.5*p*v(i)^2*S*Cdprof(i);

%Induced Drag Coefficient
Cdi(i)=(Cl(i)^2)/(pi*e*AR);
Dwi(i)=0.5*p*v(i)^2*S*Cdi(i);

%Total Drag Coefficient for the Wing
Cd(i)=Cdprof(i)+Cdi(i);
%Total Wing Drag
Dw(i)=0.5*p*v(i)^2*S*Cd(i);

%Profile Drag Coefficient Vertical Tail
if ReVT(i)>=300000 && ReVT(i)<400000
```

```
    Cdprofvt1(i)=interp1(ClRe300T,CdRe300T,0);
    Cdprofvt2(i)=interp1(ClRe400T,CdRe400T,0);
    Cdprofvt(i)=exp((log(Cdprofvt1(i))+log(Cdprofvt2(i)))/2);
elseif ReVT(i)>=400000 && ReVT(i)<500000
    Cdprofvt1(i)=interp1(ClRe400T,CdRe400T,0);
    Cdprofvt2(i)=interp1(ClRe500T,CdRe500T,0);
    Cdprofvt(i)=exp((log(Cdprofvt1(i))+log(Cdprofvt2(i)))/2);
elseif ReVT(i)>=500000 && ReVT(i)<700000
    Cdprofvt1(i)=interp1(ClRe500T,CdRe500T,0);
    Cdprofvt2(i)=interp1(ClRe700T,CdRe700T,0);
    Cdprofvt(i)=exp((log(Cdprofvt1(i))+log(Cdprofvt2(i)))/2);
elseif ReVT(i)>=700000 && ReVT(i)<1000000
    Cdprofvt1(i)=interp1(ClRe700T,CdRe700T,0);
    Cdprofvt2(i)=interp1(ClRe1000T,CdRe1000T,0);
    Cdprofvt(i)=exp((log(Cdprofvt1(i))+log(Cdprofvt2(i)))/2);
elseif ReVT(i)>=1000000 && ReVT(i)<1500000
    Cdprofvt1(i)=interp1(ClRe1000T,CdRe1000T,0);
    Cdprofvt2(i)=interp1(ClRe1500T,CdRe1500T,0);
    Cdprofvt(i)=exp((log(Cdprofvt1(i))+log(Cdprofvt2(i)))/2);
elseif ReVT(i)>=1500000 && ReVT(i)<2000000
    Cdprofvt1(i)=interp1(ClRe1500T,CdRe1500T,0);
    Cdprofvt2(i)=interp1(ClRe2000T,CdRe2000T,0);
    Cdprofvt(i)=exp((log(Cdprofvt1(i))+log(Cdprofvt2(i)))/2);
elseif ReVT(i)>=2000000 && ReVT(i)<4000000
    Cdprofvt1(i)=interp1(ClRe2000T,CdRe2000T,0);
    Cdprofvt2(i)=interp1(ClRe4000T,CdRe4000T,0);
    Cdprofvt(i)=exp((log(Cdprofvt1(i))+log(Cdprofvt2(i)))/2);
elseif ReVT(i)>=4000000 && ReVT(i)<6000000
    Cdprofvt1(i)=interp1(ClRe4000T,CdRe4000T,0);
    Cdprofvt2(i)=interp1(ClRe6000T,CdRe6000T,0);
    Cdprofvt(i)=exp((log(Cdprofvt1(i))+log(Cdprofvt2(i)))/2);
end

%Profile Drag Horizontal Tail
if ReHT(i)>=300000 && ReHT(i)<400000
    Cdprofht1(i)=interp1(ClRe300T,CdRe300T,0);
    Cdprofht2(i)=interp1(ClRe400T,CdRe400T,0);
    Cdprofht(i)=exp((log(Cdprofht1(i))+log(Cdprofht2(i)))/2);
elseif ReHT(i)>=400000 && ReHT(i)<500000
    Cdprofht1(i)=interp1(ClRe400T,CdRe400T,0);
    Cdprofht2(i)=interp1(ClRe500T,CdRe500T,0);
    Cdprofht(i)=exp((log(Cdprofht1(i))+log(Cdprofht2(i)))/2);
elseif ReHT(i)>=500000 && ReHT(i)<700000
    Cdprofht1(i)=interp1(ClRe500T,CdRe500T,0);
    Cdprofht2(i)=interp1(ClRe700T,CdRe700T,0);
    Cdprofht(i)=exp((log(Cdprofht1(i))+log(Cdprofht2(i)))/2);
elseif ReHT(i)>=700000 && ReHT(i)<1000000
    Cdprofht1(i)=interp1(ClRe700T,CdRe700T,0);
    Cdprofht2(i)=interp1(ClRe1000T,CdRe1000T,0);
    Cdprofht(i)=exp((log(Cdprofht1(i))+log(Cdprofht2(i)))/2);
elseif ReHT(i)>=1000000 && ReHT(i)<1500000
    Cdprofht1(i)=interp1(ClRe1000T,CdRe1000T,0);
    Cdprofht2(i)=interp1(ClRe1500T,CdRe1500T,0);
    Cdprofht(i)=exp((log(Cdprofht1(i))+log(Cdprofht2(i)))/2);
elseif ReHT(i)>=1500000 && ReHT(i)<2000000
```

```
        Cdprofht1(i)=interp1(ClRe1500T,CdRe1500T,0);
        Cdprofht2(i)=interp1(ClRe2000T,CdRe2000T,0);
        Cdprofht(i)=exp((log(Cdprofht1(i))+log(Cdprofht2(i)))/2);
    elseif ReHT(i)>=2000000 && ReHT(i)<4000000
        Cdprofht1(i)=interp1(ClRe2000T,CdRe2000T,0);
        Cdprofht2(i)=interp1(ClRe4000T,CdRe4000T,0);
        Cdprofht(i)=exp((log(Cdprofht1(i))+log(Cdprofht2(i)))/2);
    elseif ReHT(i)>=4000000 && ReHT(i)<6000000
        Cdprofht1(i)=interp1(ClRe4000T,CdRe4000T,0);
        Cdprofht2(i)=interp1(ClRe6000T,CdRe6000T,0);
        Cdprofht(i)=exp((log(Cdprofht1(i))+log(Cdprofht2(i)))/2);
    end

    %Drag Horizontal Tail
    Cdht(i)=Cdprofht(i)+Cd(i);
    Dht(i)=0.5*p*v(i)^2*Sht*Cdht(i);

    %Drag Vertical Tail
    Cdvt(i)=Cdprofvt(i);
    Dvt(i)=0.5*p*v(i)^2*Svt*Cdvt(i);

    %Fuselage Drag
    for j=1:6
        Rex(j)=(p*v(i)*((i-1)+0.5))/u;
        if Rex(j)<500000
            Cfx(j)=0.664/sqrt(Rex(j));
        else
            %Cfx(j)=0.0576*Rex(j)^-0.2;
            Cfx(j)=(2*log10(Rex(j))-0.65)^-2.3;
        end
        Fj(j)=A(j)*Cfx(j);

    end

    Df(i)=0.5*p*v(i)^2*sum(Fj);

    %Interference Drag
    Dint(i)=(Dw(i)+Dht(i)+Dvt(i)+Df(i))*0.05;
    %Total Drag
    D(i)=Dw(i)+Dht(i)+Dvt(i)+Df(i)+Dint(i);

    %L/D
    LD(i)=W/D(i);
    Vsink(i)=-(1/LD(i))*v(i);
end

Dmin=min(D)*cnv;
LDmax=W/min(D);

return;
```

Appendix B

Stability and Control Equations

Table B-1. Longitudinal Stability Equations

$C_{Xu} = -2C_{D0}$	$C_{Zu} = 0$	$C_{Mu} = 0$
$C_{X\alpha} = C_{L0} + a\alpha_0 - \frac{2aC_{L0}}{\pi e_0 AR}$	$C_{Z\alpha} = -a - C_{D0} - \frac{2C_{L0}a\alpha_0}{\pi e_0 AR}$	$C_{M\alpha} = a(h - h_n)$
$C_{Xq} = 0$	$C_{Zq} = -2a_t V_H$	$C_{Mq} = -2a_t V_H \frac{l_t}{c}$
$C_{X\alpha,dot} = 0$	$C_{Z\alpha,dot} = -2a_t V_H \frac{\partial \epsilon}{\partial \alpha}$	$C_{M\alpha,dot} = -2a_t V_H \frac{l_t}{c}\frac{\partial \epsilon}{\partial \alpha}$
$C_{X\delta_e} = 0$	$C_{Z\delta_e} = -a_e \frac{S_{HT}}{S}$	$C_{M\delta_e} = -a_e V_H$

The equations above are from Etkin (2) and modified with assumptions that Mach effects are negligible.

Table B-2. Lateral Dimensional Equations

$Y_v = \frac{1}{2}\rho u_0 SC_{Y\beta}$	$L_v = \frac{1}{2}\rho u_0 bSC_{L\beta}$	$N_v = \frac{1}{2}\rho u_0 bSC_{N\beta}$
$Y_p = \frac{1}{4}\rho u_0 SbC_{Yp}$	$L_p = \frac{1}{4}\rho u_0 Sb^2 C_{Lp}$	$N_p = \frac{1}{4}\rho u_0 Sb^2 C_{Np}$
$Y_r = \frac{1}{4}\rho u_0 SbC_{Yr}$	$L_r = \frac{1}{4}\rho u_0 Sb^2 C_{Lr}$	$N_r = \frac{1}{4}\rho u_0 Sb^2 C_{Nr}$
$Y_{\delta_a} = \frac{1}{2}\rho u_0^2 SC_{Y\delta_a}$	$L_{\delta_a} = \frac{1}{2}\rho u_0^2 bSC_{L\delta_a}$	$N_{\delta_a} = \frac{1}{2}\rho u_0^2 bSC_{N\delta_a}$
$Y_{\delta_r} = \frac{1}{2}\rho u_0^2 SC_{Y\delta_r}$	$L_{\delta_r} = \frac{1}{2}\rho u_0^2 bSC_{L\delta_r}$	$N_{\delta_r} = \frac{1}{2}\rho u_0^2 bSC_{N\delta_r}$

REFERENCES

1. Abbott, Allan V., and David Gordon Wilson. *Human-powered Vehicles*. Champaign, IL: Human Kinetics, 1995.
2. Beron-Rawdon, B. "Dihedral", Model Aviation Magazine, August through November 1988.
3. Etkin, B., and Reid, L. D., *Dynamics of Flight: Stability and Control*, 3rd ed., John Wiley & Sons, Inc., Danvers, MA, 1996, Chaps. 3, 5, 6.
4. Finck, R. D., and D. E. Hoak. *USAF Stability and Control Datcom*. Irvine, CA: Global Engineering Documents, 1978.
5. Jex, H. R., and Mitchell, D. G., "Stability and Control of the Gossamer Human-Powered Aircraft by Analysis and Flight Test," CONTRACT NAS4-2705, 1982.
6. McCormick, B., *Aerodynamics, Aeronautics, and Flight Mechanics*, 2nd ed., John Wiley & Sons, Inc., Danvers, MA, 1995. Chaps. 4, 9.
7. Morelli, Piero. *Static Stability and Control of Sailplanes*. Voorburg, The Netherlands: Organisation Scientifique Et Technique Internationale Du Vol à Voile, 1976.
8. Royal Aeronautical Society, "Human Powered" *Kremer Competitions* [online database], URL: http://aerosociety.com/About-Us/specgroups/Human-Powered/Kremer [cited 25 March 2013].
9. Thomas, F., *Fundamentals of Sailplane Design*, translated by J. Milgram, College Park Press, College Park, MA, 1999, pp. 48-61.

ACADEMIC VITA

Peter Michael Blasco

pmb5110@psu.edu

PO Box 866
Sherwood, OR 97140

Education

B.S., Aerospace Engineering, 2013, The Pennsylvania State University, University Park, PA

Honors and Awards

- Dean's List, all semesters
- Sigma Gamma Tau member
- Victor Simon Memorial Scholarship recipient
- First place winner, College of Engineering Research Symposium poster competition

Association Memberships/Activities

- Theta Chi Fraternity, former Secretary, former Scholarship Chair, Service Chair
- Penn State Aviation Club, Vice President
- American Institute of Aeronautics and Astronautics, Student member

Research Interests

I am fascinated by aircraft performance, stability and control, and design. My main focus for graduate research is aircraft stability and control, but I'm not opposed to looking into research in other areas such as design optimization and applied aerodynamics. One area of interest for me is how the control systems of an aircraft and pilot interaction may change in the future. Researching

new ways to approach the relationship between pilot interaction and control of a complex dynamically unstable aircraft would be a profound and challenging field of study.

Publications and Papers

Stability and Control of a Human Powered Aircraft, 2013 AIAA Student Conference